IRWIN AND JOAN JACOBS
CENTER FOR COMMUNICATION AND INFORMATION TECHNOLOGIES

The neuronal response at extended timescales: long-term correlations without long-term memory

Daniel Soudry and Ron Meir

CCIT Report #848
December 2013

DEPARTMENT OF ELECTRICAL ENGINEERING
TECHNION - ISRAEL INSTITUTE OF TECHNOLOGY, HAIFA 32000, ISRAEL

CCIT Report #848 December 2013

The neuronal response at extended timescales: long-term correlations without long-term memory

Daniel Soudry and Ron Meir

December 20, 2013

Department of Electrical Engineering, the Laboratory for Network Biology Research, Technion 32000, Haifa , Israel

Abstract

Long term temporal correlations frequently appear at many levels of neural activity. We show that when such correlations appear in isolated neurons, they indicate the existence of slow underlying processes and lead to explicit conditions on the dynamics of these processes. Moreover, although these slow processes can potentially store information for long times, we demonstrate that this does not imply that the neuron possesses a long memory of its input, even if these processes are bidirectionally coupled with neuronal response. We derive these results for a broad class of biophysical neuron models, and then fit a specific model to recent experiments. The model reproduces the experimental results, exhibiting long term (days-long) correlations due to the interaction between slow variables and internal fluctuations. However, its memory of the input decays on a timescale of minutes. We suggest experiments to test these predictions directly.

1 Introduction

Long term temporal correlations, or "$f^{-\alpha}$ statistics" [22], are ubiquitously found at multiple levels of brain and behavior [50, and refrences therein]. For example, $f^{-\alpha}$ statistics appear in human cognition [14, 40], brain and network activity (measured using electroencephalograph or local field potentials [3, and refrences therin]), and even Action Potentials (APs) generated by single neurons [30, 11]. The presence of these long correlations in a neuron's AP responses suggests it is affected by processes with slow dynamics, which can retain information for long times. As a result, if these slow processes are also affected by APs, then the generation of each AP (indirectly) depends on a rather long history of the neuron's previous inputs and APs. This potentially allows a single neuron to perform complex computations over very long timescales. However, it remains unclear whether this type of computation indeed occurs.

Cortical neurons indeed contain processes taking place on multiple timescales. Many types of ion channels are known, with a large range of kinetic rates [1]. Additional new sub-cellular kinetic processes are being discovered at an explosive rate [2, 44, 9]. This variety is particularly large for very slow processes [29]. Such rich biophysical machinery

can potentially modulate the generation of Action Potentials (APs) on long timescales. Evidence for such abilities was observed in recent works, which investigated how cortical neurons temporally integrate noisy current stimuli [27, 26, 39]. The temporal integration of the input was approximated using filters with power law decay, reflecting "long memory". However, these filters were fitted only up to a timescale of about 10 sec (or equivalently, frequencies smaller than 10^{-1} Hz), possibly due to the limited duration of the experiments, which involve intracellular recording.

This raises the question - would the neuron still have long memory on timescales longer than 10 sec? Generally, the answer may depend on the type of stimulus used. For example, certain ion channels may "remember" non-sparse inputs longer than sparse inputs [47]. Here, we focus on the case of the sparse (AP-like) input (Fig. 1), imitating the "natural" input for an axonal compartment which receives APs from a previous compartment. Such stimulation is used in various experiments (*e.g.*, [17, 8, 11]).

We find general conditions under which a neuron can generate $f^{-\alpha}$ statistics in its spiking activity, and show that this does not imply that a neuron has long memory of its history. Specifically, in order to generate $f^{-\alpha}$ statistics slow processes should span a wide range of timescales with slower processes having a higher level of internally generated fluctuations (*e.g.*, more "noisy", due to lower ion channel numbers). However, in a minimal model that generates this behavior, slow processes do not retain memory of the input fluctuations beyond a finite "short" timescale, even though they are affected by the membrane's voltage. A main reason for this is that the "fastest adaptation process" in the model adjusts the neuron's response in such a way that any perturbation in the response is canceled out, before slower processes are affected.

We fit the minimal model to the days-long experiments in [11], where synaptically isolated individual neurons, from a rat cortical culture, were stimulated with extra-cellular sparse current pulses for an unprecedented duration of days. The neurons exhibited $f^{-\alpha}$ statistics, responding in a complex and irregular manner from seconds to days. The synaptic isolation of the neurons in the network, and their low cross-correlations indicate that these $f^{-\alpha}$ fluctuations are internally generated in the neurons (section D). We are able to reproduce their results (Fig. 3), and predict that the neuron should remember perturbations in its input for about 10^2 seconds (Fig. 4). We suggest further experiments to test these predictions (Fig. 5).

The remainder of the paper is organized as follows. We begin in section 2.1 by presenting the basic setup. Then, in section 2.2, we present the general framework for biophysical modeling of neurons. Working in this framework, in section 2.3 we recall the mathematical formalism from [46] and derive the power spectrum density for periodic input stimuli. Following a description of $f^{-\alpha}$ behavior in section 3.1, we provide in section 3.2 both general and "minimal" conditions for a neuron to display such scaling. In section 3.3 we consider the implications of the model for the input-output relation of the neuron, given general stationary inputs. In section 3.4 we demonstrate this numerically in a specific biophysical model which is fitted to the experimental results of [11]. We conclude in section 4 with a summary and discussion of our results. An extensive appendix contains many of the technical details used throughout the paper.

2 Methods

2.1 Preliminaries

In our notation $\langle\cdot\rangle$ is an ensemble average, $i \triangleq \sqrt{-1}$, a non-capital boldfaced letter $\mathbf{x} \triangleq (x_1, \ldots, x_n)^\top$ is a column vector (where $(\cdot)^\top$ denotes transpose), and a boldfaced capital letter $\mathbf{X}$ is a matrix (with components X_{mn}).

Stimulation. As in [46] we examine a single, synaptically isolated, excitable neuron under "spike" stimulation. In this stimulation regime, the stimulation current, $I(t)$, consists of a train of identical short pulses arriving at times t_m and amplitude I_0. The intervals between the stimulation times are denoted $T_m \triangleq t_{m+1} - t_m$ (Fig. 1A, *top*). We assume that the stimulation is sparse, *i.e.*, $T_m \gg \tau_{\mathrm{AP}}$, with τ_{AP} being the timescale of an AP (Fig. 1B). Since the neuron is "excitable" it does not generate APs unless stimulated, as in [11] (*i.e.*, the neuron is neither oscillatory nor spontaneously firing). However, after a stimulation the neuron can either respond with a detectable AP or not respond. We denote AP occurrences a Y_m, where $Y_m = 1$ if an AP occurred immediately after the m-th stimulation, and 0 otherwise (Fig. 1A, *bottom*). Note also that Y_m is not generally the same as the common count process generated from the APs by binning them into equally sized bins (section B.1) - unless T_m is constant and equal to the bin size.

Statistics. We assume both Y_m and T_m are wide-sense stationary [37]. We denote $p_* \triangleq \langle Y_m \rangle$ to be the mean probability to generate an AP and $T_* \triangleq \langle T_m \rangle$ as the mean stimulation period. Furthermore, we denote $\hat{Y}_m \triangleq Y_m - p_*$ and $\hat{T}_m = T_m - T_*$ as the perturbations of Y_m and T_m from their means. An important tool in quantifying the statistics of signals is the power spectral density (PSD), namely the Fourier transform of the auto-covariance [37]. For analytical convenience, in this work we will use a PSD of the form

$$S_Y(f) \triangleq T_* \sum_{k=-\infty}^{\infty} \left\langle \hat{Y}_m \hat{Y}_{m+k} \right\rangle e^{-2\pi f T_* i k}, \tag{1}$$

with $0 \leq f \ll T_*^{-1}$ in Hertz frequency units. Note that this PSD is proportional to the PSD of the common binned AP (Eq. 68), under periodical stimulus and for low frequencies - which is the regime under which we will investigate the PSD (similarly to the experiment [11]). We similarly define the PSD $S_T(f)$ and the cross-PSD $S_{YT}(f)$.

2.2 General Framework

We model the neuron in the standard framework of biophysical neural models - *i.e.*, Conductance Based Models (CBMs). However, rather than focusing only on a specific model, we establish general results about a broad class of models. In this framework, the voltage dynamics of an isopotential neuron are determined by ion channels, protein pores which change conformations stochastically with voltage-dependent rates [19]. On the population level, such dynamics are generically very well described by models of the

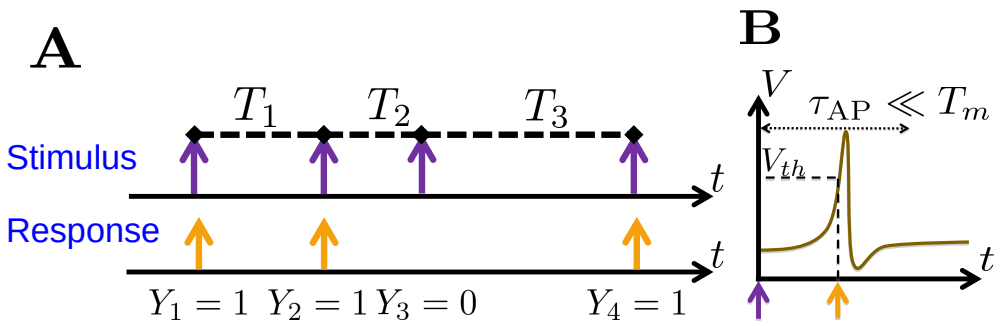

Figure 1: **Stimulation Regime.** **A** Stimulation consists of (extracellular) sparse current spikes, with inter-stimulus intervals T_m and Action Potential (AP) occurrences Y_m. **B** An AP "occurred" if the voltage V crossed a threshold V_{th} following the (sparse) stimulus, with $T_m \gg \tau_{\mathrm{AP}}$.

form of ([46], Eqs. 4-6)

$$\dot{V} = f\left(V, \mathbf{r}, \mathbf{s}, I\left(t\right)\right) \tag{2}$$

$$\dot{\mathbf{r}} = \mathbf{A}_r\left(V\right)\mathbf{r} - \mathbf{b}_r\left(V\right) + \mathbf{B}_r\left(V, \mathbf{r}\right)\boldsymbol{\xi}_r \tag{3}$$

$$\dot{\mathbf{s}} = \mathbf{A}_s\left(V\right)\mathbf{s} - \mathbf{b}_s\left(V\right) + \mathbf{B}_s\left(V, \mathbf{s}\right)\boldsymbol{\xi}_s \tag{4}$$

with **voltage** V, stimulation current $I\left(t\right)$, **rapid** variables $\mathbf{r}$ (*e.g.*, m, n, h in the Hodgkin-Huxley (HH) model [20]), **slow** "excitability" variables $\mathbf{s} \in \left[0,1\right]^M$ (e.g., slow sodium inactivation [6]), white noise processes $\boldsymbol{\xi}_{r/s}$ (with zero mean and unit variance). Also, the matrices $\mathbf{A}_{r/s}$ and the vectors $\mathbf{b}_{r/s}$ can be written explicitly using the kinetic rates of the ion channels, while the matrices $\mathbf{B}_{r/s}$ can be written using those rates in addition to ion channel numbers**.** Lastly, we denote

$$\mathbf{D}_r \triangleq \mathbf{B}_r\mathbf{B}_r^{\top} \; ; \; \mathbf{D}_s \triangleq \mathbf{B}_s\mathbf{B}_s^{\top}$$

as the diffusion matrices [35]. In these models the voltage and the rapid variables constitute the AP generation, while the slow variables modulate the excitability of the cell. For simplicity, we assumed that $\mathbf{r}$ and $\mathbf{s}$ are not coupled directly, but this is non-essential [46]. The parameter space can be constrained [48], since we consider here only *excitable* neurons which do not fire spontaneously (*non-oscillatory*) and which have a single resting state - as is common for *isolated* cortical cells, e.g., [11].

2.3 The power spectral density of the response

PSD-based estimators are central tools in quantifying long term correlations [41, 25], and are commonly used in experimental settings - as in [11]. Therefore, In this section we focus on the PSD of the neural response under sparse stimulation regime (section 2.1) of a CBM (section 2.2).

2.3.1 Recap - previous mathematical results

Typically, CBMs (Eqs. 2-4) contain many unknown parameters, and are highly non-linear. Therefore, it is quite hard to fit them using a purely simulation based approach, especially over long timescales, where simulations are long and models have more unknown parameters. Therefore, we developed a reduction method that simplifies analysis and enables fitting of such models. We refer the reader to [46] for full mathematical details.

In this method, we semi-analytically[1] reduce the full model (2-4) to a simplified model, under the assumption that the timescales of rapid and slow variables are well separated. Given another assumption, that the neuron dynamics are sufficiently "noisy", we can linearize the model dynamics, so that

$$\hat{Y}_m = p_* + \mathbf{w}^\top \left(\mathbf{s}\left(t_m\right) - \mathbf{s}_*\right) , \tag{5}$$

where p_*, $\mathbf{s}_*$ (the excitability fixed point) and w_j (an "effective weight" of component s_j,) can be found self-consistently as a function of T_*. After these quantities are found, an expression for the output PSD $S_Y\left(f\right)$ in this model can be written explicitly. We let X_+, X_- and X_0 denote the averages of the quantity X_s during an AP response, a failed AP response and rest, respectively. Also, we denote

$$X_* \triangleq \tau_{\mathrm{AP}} T_*^{-1} \left(p_* X_+ + \left(1 - p_*\right) X_-\right) + \left(1 - \tau_{\mathrm{AP}} T_*^{-1}\right) X_0$$

as the steady state mean value of X_s. For example, $\mathbf{A}_*$ and $\mathbf{D}_*$ are the respective steady state means of $\mathbf{A}_s$ and $\mathbf{D}_s$. Additionally, we denote $\sigma_e^2 \triangleq p_* - p_*^2$ as the steady state variance of Y_m,

$$\boldsymbol{a} \triangleq \tau_{\mathrm{AP}} \left(\left(\mathbf{A}_+ - \mathbf{A}_-\right) \mathbf{s}_* - \left(\mathbf{b}_+ - \mathbf{b}_-\right)\right) \tag{6}$$

as a "feedback" vector (see Fig. 1C in [46] to understand this interpretation), and

$$\mathbf{H}_c\left(f\right) \triangleq \left(2\pi f i \mathbf{I} - \mathbf{A}_* - T_*^{-1} \boldsymbol{a} \mathbf{w}^\top\right)^{-1} \tag{7}$$

as the "closed loop transfer function" (including the effect of the feedback), with $\mathbf{I}$ being the identity matrix. Using the above notation, we can derive the PSD of the response. Given a periodical stimulation ($\hat{T}_m = 0$) we obtain ([46], Eq. 14)

$$S_Y\left(f\right) = \mathbf{w}^\top \mathbf{H}_c\left(-f\right) \mathbf{D}_* \mathbf{H}_c^\top\left(f\right) \mathbf{w} + T_* \sigma_e^2 \left|1 + T_*^{-1} \mathbf{w}^\top \mathbf{H}_c\left(-f\right) \boldsymbol{a}\right|^2 . \tag{8}$$

Though Eq. 8 relies on two simplifying assumptions, extensive numerical simulations ([46], Figs. 3-4) showed that this expression is rather robust and remains accurate in many cases even if these assumptions do not hold. Therefore, in this work we will always assume that Eq. 8 is accurate.

2.3.2 The effect of feedback

In the neuron, the slow excitability variables $\mathbf{s}$ affect the response of the neuron, which, in turn, affects the dynamics of the the slow excitability variables. To simplify analysis,

[1] A semi-analytic derivation is an analytic derivation in which some terms are obtained by relatively simple numerics.

it is desirable to "isolate" this feedback effect. In order to do this, we apply the Sherman Morrison lemma to Eq. 7,

$$\mathbf{w}^\top \mathbf{H}_c(-f) = \mathbf{w}^\top \mathbf{H}_o(-f) \left(1 - T_*^{-1} \mathbf{w}^\top \mathbf{H}_o(-f)\, \boldsymbol{a}\right)^{-1},$$

with

$$\mathbf{H}_o(f) \triangleq (2\pi f i \mathbf{I} - \mathbf{A}_*)^{-1} \tag{9}$$

being the "open loop" version of $\mathbf{H}_c(f)$ (*i.e.*, if $\boldsymbol{a}$ is set to zero). Using this in Eq. 8 we obtain

$$S_Y(f) \quad = \quad S_Y^o(f) \left|\kappa(f)\right|^{-2}, \tag{10}$$

with $S_Y^o(f)$ being the "open loop" version of $S_Y(f)$ (*i.e.*, $S_Y(f)$ with $\boldsymbol{a}$ set to zero),

$$S_Y^o(f) \quad \triangleq \quad T_*\sigma_e^2 + \mathbf{w}^\top \mathbf{H}_o(-f)\, \mathbf{D}_* \mathbf{H}_o^\top(f)\, \mathbf{w} \tag{11}$$

and $\kappa(f)$ determines the effect of the feedback

$$\kappa(f) \quad \triangleq \quad 1 - T_*^{-1} \mathbf{w}^\top \mathbf{H}_o(-f)\, \boldsymbol{a}\,. \tag{12}$$

Note that $\kappa(f)$ depends on the feedback through the variable $\boldsymbol{a}$. If $\boldsymbol{a} \to 0$, for example, the kinetic rates of $\mathbf{s}$ are not sensitive to AP occurrences[2]. In that case $\kappa(f) \to 1$ and $S_Y(f) \to S_Y^o(f)$.

2.3.3 Partial fractions decomposition

In order to simplify analysis, we decompose the vector expressions in Eqs. 11-12 to partial fractions.

If $\mathbf{A}_*$ is diagonalizable, than we can write Eq. 11 as (section A.1)

$$S_Y^o(f) = T_*\sigma_e^2 + \sum_{k=1}^{M} \frac{c_k}{(2\pi f)^2 + \lambda_k^2}, \tag{13}$$

where the poles λ_k are the inverse timescales of the slow variables (the eigenvalues of $\mathbf{A}_*$), arranged from large to small according to their magnitudes ($0 < |\lambda_M| < |\lambda_{M-1}| < \cdots < |\lambda_1|$) and

$$c_k = \sum_{j=1}^{M} w_k D_{kj} w_j \frac{2\lambda_k}{\lambda_k + \lambda_j} \tag{14}$$

being the amplitude of these poles, with D_{kj} and w_k being the respective components of $\mathbf{D}_*$ and $\mathbf{w}$ in a basis in which $\mathbf{A}_*$ is diagonal. Note that, $\forall k$, $\mathrm{Re}[\lambda_k] < 0$ (from the properties of $\mathbf{A}_*$).

Using a similar derivation for $\kappa(f)$, we obtain

$$\kappa(f) \quad = \quad 1 - \sum_{k=1}^{M} \frac{T_*^{-1} w_k a_k}{2\pi f i - \lambda_k}, \tag{15}$$

with a_k and w_k being the respective components of $\boldsymbol{a}$ and $\mathbf{w}$ in a base in which $\mathbf{A}_*$ is diagonal.

[2] For example, this can happen if the kinetic rates all have low voltage threshold, resulting in $\mathbf{A}_+ \approx \mathbf{A}_-$ and $\mathbf{b}_+ \approx \mathbf{b}_-$.

2.3.4 Example - a "diagonal" model

For concreteness, we demonstrate our results on a simple model in which $\mathbf{A}_*$ is a diagonal matrix and, as a result, $\mathbf{D}_*$ (which depends on $\mathbf{A}_*$) is also diagonal. In this "diagonal" model all the components of $\mathbf{s}$ are uncoupled (*i.e.*, belong to different channel types), Eq. 4 can be written as [46, section 4.1]

$$\dot{s}_k = \delta_k(V)(1-s_k) - \gamma_k(V)\, s_k + \sigma_{s,k}(V, s_k)\, \xi_{s,k} \tag{16}$$

$\forall k \in \{1, \ldots, M\}$, where $\sigma_{s,k}(V,s) = \left[(\delta_k(V)(1-s_k) + \gamma_k(V)\, s_k)\, N_{s,k}^{-1}\right]^{1/2}$ and $N_{s,k}$ are the number of slow ion channels of type k. Similarly as before, $\gamma_{+,k}, \gamma_{-,k}$ and $\gamma_{0,k}$ denote the averages of the kinetic rate $\gamma_k(V)$ during an AP response, a failed AP response and rest, respectively. In addition

$$\gamma_{*,k} = \tau_{\mathrm{AP}} T_*^{-1} \left(p_* \gamma_{+,k} + (1-p_*)\gamma_{-,k}\right) + \left(1 - \tau_{\mathrm{AP}} T_*^{-1}\right)\gamma_{0,k}$$

is the average $\gamma_k(V)$ in steady state. We use a similar notation for δ. Therefore

$$\begin{aligned} (\mathbf{A}_*)_{kk} &= -\gamma_{*,k} - \delta_{*,k} \\ (\mathbf{D}_*)_{kk} &= \frac{1}{N_{s,k}} \frac{\gamma_{*,k}\delta_{*,k}}{\gamma_{*,k} + \delta_{*,k}} \end{aligned}$$

with zero on all other (non-diagonal) components and

$$a_k = \tau_{AP} \frac{(\gamma_* (\delta_+ - \delta_-) - (\gamma_+ - \gamma_-)\, \delta_*)}{\gamma_* + \delta_*}\,. \tag{17}$$

Therefore, in Eqs. 13-14 we have,

$$\lambda_k = -\gamma_{*,k} - \delta_{*,k} \tag{18}$$

$$c_k = w_k^2 D_{kk} = \frac{w_k^2}{N_{s,k}} \frac{\gamma_{*,k}\delta_{*,k}}{\gamma_{*,k} + \delta_{*,k}}\,. \tag{19}$$

Importantly, by tuning the parameters $M, \gamma_k(V), \delta_k(V)$, $N_{s,k}$ and w_k we seem to have complete freedom in determining λ_k, c_k and a_k (Eqs. 17-19). This, in turn, would give complete freedom in tuning $S_Y^o(f)$ and $\kappa(f)$. Therefore, it seems that for any CBM (i.e., not only diagonal models) we can find an *equivalent* diagonal model - which produces exactly the same PSD of the response.

The only caveat in the previous argument is that in non-diagonal models λ_k can be complex, but not in a diagonal model, since the kinetic rates $\gamma_k(V)$ and $\delta_k(V)$ must be real numbers. How would the situation change if some of the poles had complex values? Complex poles (*i.e.*, for which $\mathrm{Im}[\lambda_k] > 0$) always come in conjugate pairs. These pairs behave asymptotically (*i.e.*, for $2\pi f \gg |\lambda_k|$ or $2\pi f \ll |\lambda_k|$) very similarly to two real poles, with an additional "resonance" (either a bump or depression) in a narrow range in the vicinity of these poles (*i.e.*, $2\pi f \sim |\lambda_k|$) (see section A.2, or [34]).

3 Results

3.1 Background on $f^{-\alpha}$ statistics

As observed in [11], the responses of isolated neurons exhibit long-term correlations robustly[3], under sparse pulse stimulation (Fig. 1 and section 2.1). Signals with such long-term correlations are often described by the term "$f^{-\alpha}$ noise". This is because the Power Spectral Density (PSD, [37]) is a central tool in detecting and quantifying such signals [41, 25]. As the name implies, if the AP pattern Y_m is a "$f^{-\alpha}$ noise signal" then its PSD (Eq. 8) has a $f^{-\alpha}$ shape

$$S_Y(f) \propto f^{-\alpha}, \tag{20}$$

where the PSD is defined here as in Eq. 1. As is usually the case for most $f^{-\alpha}$ phenomena, Eq. 20 is true only in a certain range $f_{\min} \leq f \leq f_{\max}$, and with $0 < \alpha \leq 2$. Note also that if $\alpha > 1$, then $f_{\min} > 0$ necessarily[4]. Such $f^{-\alpha}$ behavior is considered interesting due to its "scale-free" properties, which can sometimes indicate a "long memory", as explained in the introduction. Therefore, it is interesting to ask the following questions:

1. What is the biophysical origin of the $f^{-\alpha}$ behavior?
2. Does this $f^{-\alpha}$ behavior imply that the neuron "remembers" its history on very long timescales (hours and days)?

We aim to answer the first question in section 3.2, focusing on the case of periodical stimulation $T_m = T_*$, as in [11]. The second question is addressed in section 3.3, where we examine a general sparse stimulation process T_m. Finally, in section 3.4.2 we fit a specific CBM (which is an extension of a previous CBM) so it adheres to this set of minimal constraints. We numerically reproduce the experimental results of [11] and demonstrate our predictions.

3.2 Biophysical modeling of $f^{-\alpha}$ statistics

As we explained in the Introduction, neurons contain a large variety of processes operating on slow timescales. These processes are, in many cases, not well characterized or contain unknown parameters. Therefore, it is hard to model the behavior of the neuron on slow timescales with a CBM using only simulation. With so many unknowns, an exhaustive parameter search is unfeasible[5]. Fortunately, since we derived a semi-analytic expression for the PSD (Eq. 8), starting from some initial "guess" (as to which process to include, and with what parameters), it is relatively straightforward to tune the parameters so that the CBM reproduces the experimental results (*i.e.*, by maximizing some "goodness of fit" measure).

However, even if a specific model could be found to reproduce the experimental results, it would still be unclear whether or not this is would be a "useful" model - one which can be used to infer the biophysical properties of the neuron, or its response to untested inputs. The first problem is that CBMs are highly degenerate, where different parameter

[3] *i.e.*, in all neurons for which $0 < p_* < 1$.

[4] Otherwise, $0.25 \geq p_* - p_*^2 = \left\langle \hat{Y}_m^2 \right\rangle \geq 2 \int_0^{f_{\max}} S_Y(f)\, df = \infty$, which is a contradiction.

[5] Also simulations take a long time, since experiments, as in [11], are days-long.

values can generate similar behaviors[6], so we can never be sure if the "correct" model was inferred. The second problem is that it is unclear whether a "correct" model would be generally useful - since different neurons from the same type can have very different parameters [28].

In order to address the first problem, initially, in section 3.2.1 we analyze Eq. 8, and attempt to answer a more general question - what class of CBM models can generate the experimental results? We find "rather general" sufficient conditions - *i.e.*, which, given a few assumptions, also become necessary conditions. Next, in section 3.2.2, we aim to find a "minimal" set of constraint on a CBM to fulfill theses conditions. Qualitatively, these conditions indicate that, in order to reproduce the experimental results, a general CBM must:

1. Include only a finite number of ion channels of each type (implying a stochastic model).
2. Include few slow processes with timescales "covering" the range of timescales over which $S_Y(f) \propto f^{-\alpha}$ is observed.
3. Obey a certain scaling relation (with an exponent of $1-\alpha$), implying that slower processes are more "noisy".

More detailed explanations of these conditions, and a concrete example, are provided in the following two subsections.

3.2.1 General conditions for $f^{-\alpha}$ statistics

In this section we derive general conditions on the parameters of a CBM (section 2.2) so it can generate robust $f^{-\alpha}$ statistics in $S_Y(f)$. Here, we focus on the case of sparse periodical input $T_m = T_* \gg \tau_{\mathrm{AP}}$ (as in [11]).

This analysis is based on the decomposition of the PSD $S_Y(f)$ as a ratio of $S_Y^o(f)$ and the feedback term $|\kappa(f)|^2$. Recall that $S_Y(f) \propto f^{-\alpha}$ is robustly observed for all stimulation parameters - even when p_* is near 0 or 1 (see section 3.1). Note that one can arbitrarily vary p_* by changing the stimulation parameters (such as I_0 or T_*). It is straightforward to show that when $p_* \to 0$ or $p_* \to 1$, the effect of feedback is negligible[7], and therefore $S_Y(f) \approx S_Y^o(f)$. This implies that, at least for some simulation parameters, $S_Y^o(f) \propto f^{-\alpha}$. For this reason, and for the sake of analytical simplicity, we first develop general conditions so that $S_Y^o(f) \propto f^{-\alpha}$, and later we discuss the effects of the feedback $\kappa(f)$.

Note from Eq. 13 that if M (the dimension of $\mathbf{s}$ - the number of slow processes) is finite, one can have $S_Y^o(f) \propto f^{-\alpha}$ exactly if and only if $\alpha = 0$ or 2. However, these values are far from what was measured experimentally (Eq. 40). Therefore, $S_Y^o(f) \propto f^{-\alpha}$ can be generated exactly only in some limit (in which M is infinite), or approximately (if M is finite). Also, note that if $2\pi f \gg |\lambda_1|$, then $S_Y^o(f) - T_*\sigma_e^2 \propto f^{-2}$. Additionally, if $2\pi f \ll |\lambda_M|$, we have $S_Y^o(f) \approx$ constant. Therefore, Eq. 13 can generate $S_Y^o(f) \propto f^{-\alpha}$ with $0 < \alpha < 2$ only for $|\lambda_M| < 2\pi f < |\lambda_1|$.

[6] *e.g.*, in Eq. 14 many different parameters would give the same c_k.

[7] Near the edges, $\mathbf{w} \to 0$ (Eq. 81 in [46]), and so $\kappa(f) \to 1$.

Next, we explain when this becomes possible. For simplicity assume that in Eq. 13 $T_*\sigma_e^2$ is negligible and all the poles are real (the effect of complex poles will be discussed below). We define the following pole density

$$\rho(\lambda) \triangleq \sum_{k=1}^{M} c_k \delta(\lambda - \lambda_k) \tag{21}$$

where $\delta(\cdot)$ is Dirac's delta function. Using Eqs. 13 and 21 we obtain

$$S_Y^o(f) = \int \frac{\rho(\lambda)\, d\lambda}{(2\pi f)^2 + \lambda^2}. \tag{22}$$

For $|\lambda_M| \ll 2\pi f \ll |\lambda_1|$ and $0 < \alpha < 2$, Eq. 22 becomes

$$S_Y^o(f) = C f^{-\alpha} \tag{23}$$

if and **only** if (section A.3)

$$\rho(\lambda) = \rho_0 |\lambda|^{1-\alpha} \tag{24}$$

in the range $|\lambda_1| > |\lambda| > |\lambda_M|$, with $\rho_0 = 2\pi^{-1} C \sin(\pi\alpha/2)$. Therefore, $\rho(\lambda)$, the distribution of the poles, must scale similarly to $S_Y^o(f)$ (but with a different exponent).

Several comments are in order at this point.

1. It was previously known that, in a linear system, a $f^{-\alpha}$ PSD could be generated using a similarly scaled sum of real poles [21, 22]. The novelty here is two-fold: (1) Quantitatively analyzing the PSD of CBMs (which are highly non-linear) in a similar way (through Eq. 8) (2) Finding that condition 24 is not only sufficient, but necessary.

2. Formally, Eq. 24 can be exact only in the continuum limit where the the number poles is infinite and they are closely packed. However, in practice, Eq. 23 remains a rather accurate approximation even if the poles are few and well separated (Fig. 2A), as we shall demonstrate in the next section (as in [21, 22]). Clearly, for simulation purposes, it is beneficial to use a CBM with a finite number of (preferably, few) poles .

3. We have assumed that all the poles are real. What happens if some of the poles are complex? Recall (section 2.3.4) that if some poles have complex values then $S_Y^o(f)$ also has "resonances" (bumps or depressions) in a narrow range near these poles. Technically, scaling these resonance peaks can also be used to approximate Eq. 23 (Fig. 2B). However, we did not pursue this method here since it would require significantly more poles and would be much harder to implement.

4. Note that so far we have discussed only $S_Y^o(f)$. One can perform a similar analysis directly on $S_Y(f)$. However, we find it is easier to first simplify $\kappa(f)$ and then use Eq. 10. From Eq. 10 the PSD $S_Y(f)$ will have a power-law shape in the range $|\lambda_M| \ll 2\pi f \ll |\lambda_1|$ if, in that range: either (1) the magnitude of $\kappa(f)$ is constant or slowly varying, or (2) $\kappa(f)$ also has a power-law shape. In the first case the exponent of $S_Y(f)$ will be the same as the exponent of $S_Y^o(f)$, and in the second case the exponent will differ. The conditions for both cases can be derived similarly to our analysis of $S_Y^o(f)$. We demonstrate this next, in a more specific context.

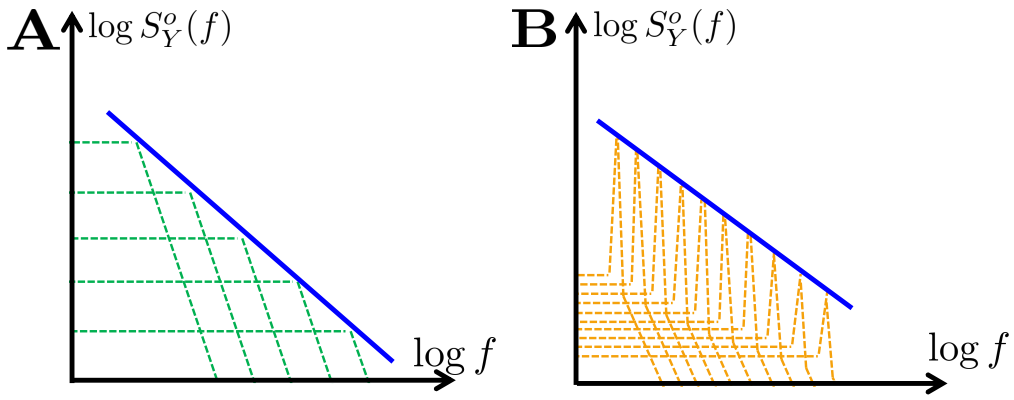

Figure 2: **Generating $f^{-\alpha}$ PSD using a finite number of poles - a graphic description.** Using partial fraction decomposition (Eq. 13) $S_Y^o(f) \propto f^{-\alpha}$ (blue) can be approximated (on a log-log scale) in two distinct ways: **A** Using a sum of a real poles (green), with scaled amplitudes (approximating Eq. 24) **B** Using a sum of complex poles (orange), with scaled "resonance peaks" (Eq. 44). In this work we focus on the first case (A), since it is simpler and requires much fewer poles.

3.2.2 A minimal model for $f^{-\alpha}$ statistics

In the previous section we found general conditions under which Eq. 11 gives $S_Y^o(f) \propto f^{-\alpha}$. In this section, we aim is to generate $S_Y^o(f) \propto f^{-\alpha}$ over $f_{\min} < f < f_{\max}$ in a minimal model, in which M (the dimension of $\mathbf{s}$) is as small as possible. As explained in section 2.3.4 we do not lose any relevant generality if we restrict ourselves to the case where $\mathbf{A}_*$ is diagonal (Eq. 16). From Eq. 24, we know that $|\lambda_k|$ must "cover" the frequency range $f_{\min} < f < f_{\max}$. In order for M to be small, we choose λ_k to be uniform over a logarithmic scale (similarly to [22]), so $\lambda_k \propto \epsilon^k$ with $\epsilon < 1$. The "simplest" way to achieve this is to have (see Eq. 16)

$$\gamma_k(V) = \gamma_1(V)\,\epsilon^{k-1} \quad ; \quad \delta_k(V) = \delta_1(V)\,\epsilon^{k-1} \tag{25}$$

so

$$\lambda_k \;=\; \lambda_1 \epsilon^{k-1}\,. \tag{26}$$

In order for $\lambda_k/(2\pi)$ to cover the range $[f_{\min}, f_{\max}]$ we require that

$$|\lambda_1| > 2\pi f_{\max}\ ;\ |\lambda_M| = |\lambda_1|\,\epsilon^{M-1} \ll 2\pi f_{\min}\,. \tag{27}$$

Given M, this sets a constraint on ϵ. In order to have scaling in $\rho(\lambda)$, as in Eq. 24, we also require that $c_k \propto |\lambda|^{1-\alpha}\, d\lambda \propto \epsilon^{(2-\alpha)k}$, since $d\lambda = \lambda_k - \lambda_{k-1} \propto \epsilon^k$. Therefore, from Eqs. 19 and 18 we have

$$\frac{w_k^2}{N_{s,k}} \propto \epsilon^{(1-\alpha)k}\,.$$

so that $S_Y^o(f) \propto f^{-\alpha}$. Therefore, we require that $w_k \propto \epsilon^{-\mu k}$, $N_{s,k} \propto \epsilon^{\nu k}$ with $2\mu + \nu = \alpha - 1$. For $\mu > 0$ the slower processes (larger k) have larger weight. For $\nu > 0$ slower processes have a smaller number of ion channels (therefore, they are more "noisy").

In section A.4, we investigate what type of scaling will generate also $S_Y(f) \propto f^{-\alpha}$, taking into account the effects of feedback (through $\kappa(f)$). We conclude that, because of the feedback, a value of $\mu > 0$ would not change the exponent of $S_Y(f)$ over a "reasonable" range of parameters (*i.e.*, assuming $\nu > -2$). Therefore, the simplest way to generate $S_Y(f) \propto f^{-\alpha}$ would be to take $\mu = 0$. In this case, we have (Eq. 57), for $-1 < \nu < 1$ and $|\lambda_M| \ll 2\pi f \ll |\lambda_1|$,

$$S_Y(f) \propto \frac{1}{N_{s,1}} \frac{f^{-(1+\nu)}}{\ln^2 f}, \tag{28}$$

where the logarithmic correction arises from the effect of feedback $\kappa(f)$. A few comments on Eq. 28 are in order at this point.

1. Due to the logarithmic correction, in order to approximate $S_Y(f) \propto f^{-\alpha}$ it is a reasonable choice to set ν slightly higher than $\alpha - 1$, *e.g.*,

$$\nu = \alpha - 0.9. \tag{29}$$

2. Even if there is no scaling in the parameters (*i.e.*, $\mu = \nu = 0$), we obtain $S_Y(f) \propto f^{-1}$ (neglecting logarithmic factors).

3. Eq. 28 is based on asymptotic derivation, which is correct in two opposing limits ("sparse" or "dense" poles, section A.5), indicating that these results are rather robust to parameter perturbations.

4. The magnitude of the ion channels number $N_{s,1}$ is inversely proportional to the magnitude of $S_Y(f)$ (*i.e.*, its proportionality constant), while the value w_1 (the magnitude of the weights) does not affect $S_Y(f)$.

5. When $N_{s,1} \to \infty$ we have $S_Y(f) \to 0$, implying that in the deterministic limit, such a CBM does not generate $f^{-\alpha}$ noise (in accordance with our results from [48]).

3.3 The input-output relation of the neuron

In the previous section we derived minimal biophysical constraints under which a neuron may generate $f^{-\alpha}$ statistics in response to periodic stimulation. In this section we explore the input-output relation of the neuron under these constraints, in the case where the inter-stimulus intervals T_m form a general (sparse) random process. We decompose the neuronal response into contributions from its "long" history of internal fluctuations and its "short" history of inputs, quantifying neuronal memory.

3.3.1 The linearized input-output relation

Recall that $\hat{T}_m \triangleq T_m - T_*$, with $T_* \triangleq \langle T_m \rangle$ and $S_T(f)$ the PSD of T_m. As explained in [46], for a *general* CBM[8] we can decompose $\hat{Y}_m$, the fluctuations in the neuronal response,

[8] *i.e.*, Eqs. 2-4, with the same assumptions as we had in section 2.3.1.

to a linear sum of the history of the input and internal noise, *i.e.*,

$$\hat{Y}_m = \sum_{k=0}^{\infty} h_k^{\text{ext}} \hat{T}_{m-k} + \sum_{k=0}^{\infty} h_k^{\text{int}} z_{m-k} \,, \tag{30}$$

with the filter h_k^{ext} used to integrate *external* fluctuations in the inputs, and the filter h_k^{int} used to integrate z_m, a zero mean and unit variance white noise representing *internal* fluctuations (*e.g.*, ion channel noise). It is easier to analyze this I/O in the frequency domain, where Eq. 30 becomes ([46], Eq. 18)

$$\hat{Y}(f) = H^{\text{ext}}(f)\,\hat{T}(f) + H^{\text{int}}(f)\,z(f) \,, \tag{31}$$

where we define $X(f)$ to be the Fourier transform of $X(t)$. Together, $H^{\text{ext}}(f)$ and $H^{\text{int}}(f)$) describe the $\hat{T}_m \to \hat{Y}_m$ neuronal I/O at very long timescales.

Note that these filters are related to the PSDs, in the following way

$$S_{YT}(f) = H^{\text{ext}}(-f)\,S_T(f) \,, \tag{32}$$

$$S_Y(f) = \left|H^{\text{ext}}(f)\right|^2 S_T(f) + \left|H^{\text{int}}(f)\right|^2 . \tag{33}$$

Notably, from Eq. 33, if the input to the neuron is not periodical (so, $S_T(f) \neq 0$), then the PSD $S_Y(f)$ should be the same as calculated previously, except for the addition of $\left|H^{\text{ext}}(f)\right|^2 S_T(f)$.

3.3.2 The shape of the input-output filters

For a general CBM, we can derive semi-analytically the exact form of the filters in Eq. 31 from its parameters, as we did for $S_Y(f)$. For example, if $\hat{T}_m = 0$ (periodical input), then also $S_T(f) = 0$, and so

$$\left|H_{\text{int}}(f)\right|^2 = S_Y(f) \,, \tag{34}$$

where $S_Y(f)$ is the PSD we derived previously (Eq. 8). Additionally, we obtain ([46], Eq. 16)

$$H^{\text{ext}}(f) = T_*^{-1}\mathbf{w}^\top \mathbf{H}_c(f)\,\mathbf{d} \,. \tag{35}$$

with

$$\mathbf{d} \triangleq \mathbf{A}_0\mathbf{s}_* - \mathbf{b}_0. \tag{36}$$

Next, we find both filters for the minimal model described in section 3.2.2. Recall that in this model

$$w_k = w_1 \,;\, a_k \propto \epsilon^k \,;\, d_k \propto \epsilon^k \tag{37}$$

with a_1 and d_1 respectively given by Eqs. 6 and 36. To simplify analysis, we derive an asymptotic form for both filters, for the cases $|\lambda_M| \ll 2\pi f \ll |\lambda_1|$ and $2\pi f \gg |\lambda_1|$. First, from Eq. 34, and Eq. 57, we find

$$\left|H_{\text{int}}(f)\right| \sim \begin{cases} f^{-\alpha/2}/\ln f & ,\text{if } |\lambda_M| \ll 2\pi f \ll |\lambda_1| \\ \text{constant} & ,\text{if } 2\pi f \gg |\lambda_1| \end{cases} . \tag{38}$$

Similarly, from Eq. 35, we find (section A.6)

$$H^{\text{ext}}(f) \approx \frac{qd_1}{2\pi f i - qa_1} \,. \tag{39}$$

where $q \triangleq (1-\epsilon)^{-1} T_*^{-1} w_1$. A few comments on Eqs. 38-39 are in order at this point.

1. We found that $H^{\text{ext}}(f)$ is a low pass filter with a pole at $f_{\text{ext}} = qa_1/2\pi$ while $H^{\text{int}}(f) \sim f^{-\alpha/2}$ for $2\pi f \ll |\lambda_1|$. Consequently, in the temporal domain (Eq. 30), for large t (*i.e.*, large k), the neuron's memory of its external input decays exponentially ($h_k^{\text{ext}} \sim e^{-f_1 T_* k}$), while its memory of its internal fluctuations decays as a power law ($h_k^{\text{int}} \sim k^{-(1-\alpha/2)}$). Therefore, the input memory has a finite timescale (equal to f_{ext}^{-1}), while the memory of internal fluctuations is "long" (with a cutoff only near $f_{\min}^{-1}$).

2. It is perhaps surprising that Eq. 35, which has multiple poles, becomes a low pass filter with a single pole f_1. The derivation (section A.6) gives two main reasons for this. First, the scaling of w_k and d_k in Eq. 37 induces only a weak (logarithmic) scaling of the poles in open-loop. Second, even this weak scaling is canceled by the affects of the feedback.

3. Naturally, other models may have a different shape of $H^{\text{ext}}(f)$. This could be probed directly, as we explain later, in section **3.4.3**.

3.4 Modeling experimental results

In this section we apply our results to experimental data, described in section 3.4.1. In section 3.4.2 we implement the set of "minimal constraints" we found in section 3.2.2 in a specific CBM, and fit it to experimental data in which $S_Y(f) \propto f^{-\alpha}$. The analytical results in section 3.2 suggest that this specific CBM is a "reasonable" representative of the family of CBMs that can generate the experimental results. Other members of this family can be reached by varying the parameters within the (either minimal or general) constraints. Next, in section 3.4.3 we use our results from section 3.3.2 on the fitted model. We show that, although internal fluctuations in the model can affect the neural response on a timescale of days, the memory of the input is only retained for a duration of minutes. We suggest specific experiments to test this prediction. In section 3.4.4 we suggest further predictions

3.4.1 Experimental details

The experiment from [11], where a single *synaptically isolated* neuron, residing in a culture of rat cortical neurons, is stimulated periodically with a train of extracellular short current pulses with constant amplitude I_0. The observed neuronal response was characterized by different modes ([11], Fig 2). We focus on the "intermittent mode" steady state, in which $0 < p_* < 1$ (*i.e.*, sometimes the stimulation evokes an AP, and sometimes it does not). The patterns observed in Y_m, the AP occurrences timeseries, are rather irregular ([11], Fig. 2E), span multiple timescales ([11], Fig. 5) and variable (*i.e.*, patterns are not repeatable [11], Fig. 9A). More quantitatively, as indicated by the analysis ([11], Fig. 6), for *all* intermittently firing neurons, the patterns in Y_m fall into the category of "$f^{-\alpha}$ noise" where the value of α varied significantly between neurons - with

$$\alpha = 1.43 \pm 0.35 \tag{40}$$

(mean±SD). As we explained in section 3.1, this $f^{-\alpha}$ behavior is true only in some limited range $f_{\min} < f < f_{\max}$. From the experimental data, (Fig. 6C in [11]) it can be estimated that $f_{\min} < 10^{-5}$Hz and $f_{\max} \sim 10^{-2}$Hz. Also, since $\alpha > 1$, then $0 < f_{\min}$ (see section 3.1).

3.4.2 The HHMS model - a biophysical implementation of the minimal constraints

In our previous work [48] we already fitted a model that fits many of the "mean" properties of the neuronal response (*e.g.*, firing modes, transients and firing rate). This model is an extension of the original Hodgkin-Huxley model which includes Slow sodium inactivation [6, 10] (The HHS model, see section C.1). In order to maintain this fit with the experimental results, we extend the HHS model with additional slow components, obeying Eq. 16. We denote this as the HHMS model (Hodgkin Huxley model with Many Slow variables, section C.2). The equations are identical to the HHS model, except that in the voltage equation (Eq. 71) $\bar{g}_{Na} s$ is replaced by $\bar{g}_{Na} M^{-1} \sum_{i=1}^{M} s_i$, where s_1 has the same equation as s in the HHS model (Eq. 75). By symmetry, this gives identical weights to component s_i (*i.e.*, $\forall k : w_k = w_1$). The remaining rates (for $k \geq 2$) are chosen according to our constraints, so $\gamma_k(V) = \gamma(V)\epsilon^{k-1}$, $\delta_k(V) = \delta(V)\epsilon^{k-1}$ (as in Eq. 25), where $\gamma(V)$ and $\delta(V)$ are taken from the HHS model (Eq. 75) and also $N_{s,k} = N_s \epsilon^{\nu k}$. Therefore, the only free parameters are ϵ, M, N_s, ν and I_0 (I_0 is the current amplitude of the stimulation pulses).

This model can be used to fit the experimental results for any $\alpha \in [0, 2)$. We performed a numerical simulation of the full equations (Eqs. 2-4) of the HHMS model under periodical stimulation with $T_* = 50\,\text{msec}$. We aimed to fit experiment from [11], which had a similar stimulation and exhibited $S_Y(f) \sim f^{-\alpha}$, with $\alpha = 1.4$ (which is approximately the average α value measured in [11]). The current amplitude I_0 was set to $I_0 = 7.7\,\mu A$ so that the model would have the same mean response probability $p_* \approx 0.4$ as in the experimental data (using the self consistent equations for p_* from [46]). We chose $M = 5$ and $\epsilon = 0.2$ in order to satisfy constraint Eq. 27 with a minimal M. We chose $\nu = 0.5$ to satisfy Eq. 29. Lastly, we chose $N_s = 10^4$ in order to fit the magnitude of the $S_Y(f)$. This reproduced all the scaling relations observed experimentally (Fig. 3).

3.4.3 Predictions - Probing the input-output relation of the neuron

After fitting the HHMS model to the experimental results, we can examine its resulting linearized input-output relation, described by the filters $H^{\text{ext}}(f)$ and $H^{\text{int}}(f)$ (Eq. 31). The $H^{\text{int}}(f)$ filter integrates internal fluctuations , while the $H^{\text{ext}}(f)$ filter determines how external fluctuations (in the input) affect its response.

In accordance with the asymptotic forms in Eqs. 38 and 39, we find that $H^{\text{ext}}(f)$ is a low pass filter with a pole $f_{\text{ext}} \sim 10^{-2}\text{Hz}$ (Fig. 4, green) while $H^{\text{int}}(f) \sim f^{-\alpha/2}$ for $f_{\min} < f < 10^{-2}\text{Hz}$ (Fig. 4, red) with $f_{\min} < 10^{-5}\text{Hz}$. Therefore, as explained in section 3.3.2 this model implies implies that the response of the neuron is affected by internal fluctuations over the scale of days ($\sim f_{\min}^{-1}$) or more, generating the $f^{-\alpha}$ behavior we observe in Fig. 3. However external input is remembered only for minutes ($\sim f_{\text{ext}}^{-1}$).

Next, we examine two methods which allow us to probe $H^{\text{ext}}(f)$ directly and examine these predictions.

First, a simple method to probe the external input filter $H^{\text{ext}}(f)$ is through Eq. 32. Allowing reliable estimation of $H^{\text{ext}}(f)$ in a certain frequency range requires a random process stimulation for which $|H^{\text{ext}}(f)|^2 S_T(f) \gg \left|H^{\text{int}}(f)\right|$ in that range, as explained in section B.2. To demonstrate this method we estimate $S_{TY}(f)$ from the existing experimental data taken from [12], in which $S_T(f) \sim f^{-\beta}$ (above some lower cutoff). In Fig. 5A we compare this estimation with $S_{TY}(f)$ in the HHMS model in a limited range where

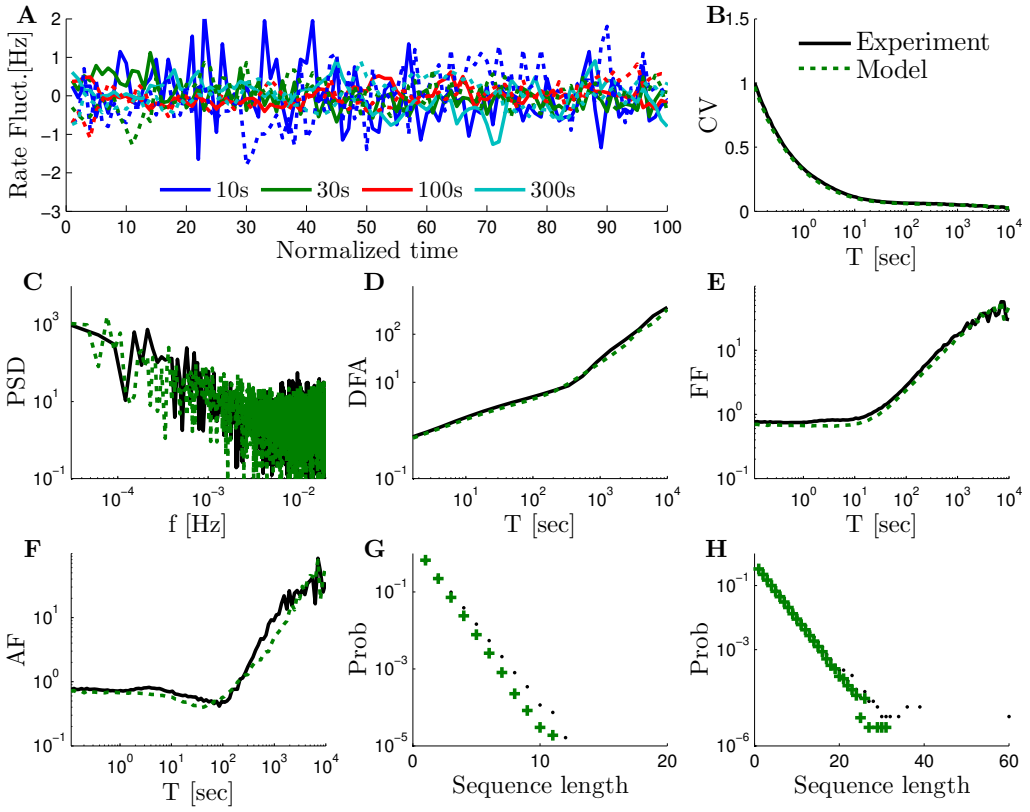

Figure 3: **The measures of "scale free" rate dynamics in the HHMS model** - comparison of the experimental data from [11] and a simulation of the extended HHS model (solid and dashed lines, respectively). We use here the same measures as in Fig. 6 in [11]: **A** The firing rate fluctuations estimated using bins of different sizes (T =10, 30, 100 and 300 sec) and plotted on a normalized time axis (units in number of bins), after subtracting the mean of each series. **B** CV of the bin counts, as a function of bin size, plotted on a log-linear axis. **C** Firing rate periodogram. **D** Detrended fluctuations analysis. **E** Fano factor (FF) curve. **F** Allan factor (AF) curve. **G** Length distribution of spike–response sequences, on a half-logarithmic axes. **H** Length distribution of no-spike-response sequences, on a double-logarithmic axes. For additional details on measures used see section B.1.

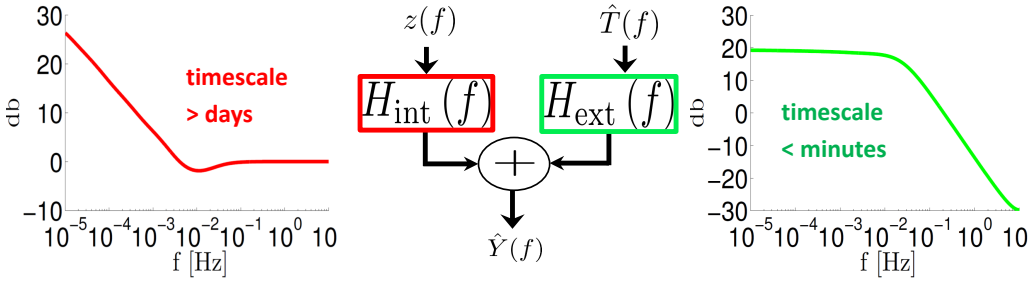

Figure 4: System decomposition into external (input - $\hat{T}(f)$) and internal (fluctuation - $z(f)$) filters. For a fitted HHMS model, $H^{\text{ext}}(f)$ is a low pass filter with cutoff $< 10^{-2}$ Hz while $H_{\text{int}}(f) \sim f^{-\alpha/2}$ for $f < 10^{-2}$ Hz.

$S_T(f)$ is sufficiently high for estimation to be accurate. It is similar to $S_{TY}(f)$ from our fitted HHMS model, validating our estimate of $H^{\text{ext}}(f)$ for that frequency range.

Second, The filter $H^{\text{ext}}(f)$ could be probed more accurately and at lower frequencies - by sinusoidally modulating the input (the internal-stimulus intervals), analogously to the sinusoidally modulated input current used in [27, 26, 39],

$$\hat{T}_m = T_{\text{amp}} \sum_{l=1}^{L} \sin\left(2\pi f_l T_* m\right) . \tag{41}$$

As we explain in section B.3, in this case the output of the neuron would be

$$\hat{Y}_m \quad = \quad \sum_{l=1}^{L} T_{\text{amp}} \left|H^{\text{ext}}(f_l)\right| \sin\left(2\pi f_l T_* m + \angle H^{\text{ext}}(f_l)\right) + \text{“noise”} .$$

This allows us to easily estimate $|H^{\text{ext}}(f)|$ using the peaks of $T_{\text{amp}}^{-1}\hat{Y}(f)$ (the Fourier transform of $T_{\text{amp}}^{-1}\hat{Y}_m$) at frequencies f_l, as we demonstrate in Fig. 5B, using our fitted HHMS model.

3.4.4 Additional Predictions

As explained in [11, 48] the latency of the AP can serve as an indicator of the cell's excitability. Specifically, this is true in the HHMS model, for periodical stimulus and $p_* = 1$, where the PSD of the latency, $S_L(f)$, is a shifted and scaled version of $S_Y(f)$ with $p_* \to 1$ (see section 4.4.6 in [46]). Therefore, in the HHMS model we also have $S_L(f) \propto f^{-\alpha}$ approximately (neglecting logarithmic factors).

Next, suppose we vary some measurable stimulation parameter, such as the mean stimulation rate T_*^{-1}. How would this affect the shape of the filters we derived? The analytical results allow us to calculate this explicitly in the HHMS model.

First, we consider the gain of the external input filter $H^{\text{ext}}(f)$ (*i.e.*, $H^{\text{ext}}(0)$). As we explain in section A.7, if $f \ll f_{\text{cutoff}}$, than

$$H^{\text{ext}}(f) \approx p_* T_*^{-1} = \bar{f}_{\text{out}} , \tag{42}$$

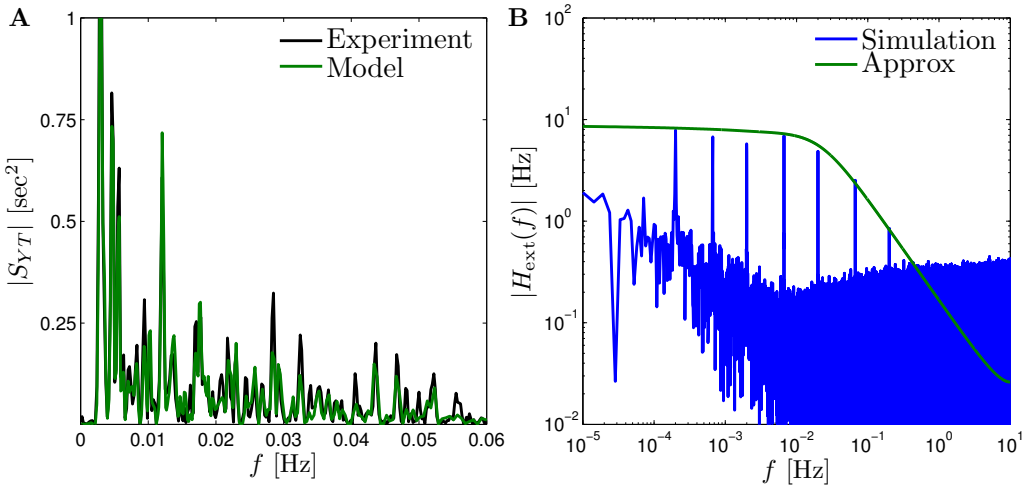

Figure 5: **Input memory in fitted model.** **(A)** Comparison of $|S_{YT}(f)|$ of the fitted model ('Model') to that estimated from the experimental confirms ('Experiment') the prediction of the input filter $|H^{\rm ext}(f)|$ for probed range. **(B)** This filter ('Approx') can be probed more accurately by peaks of $\hat{Y}(f)$ ('Simulation'), by applying a "sum of sines" input (Eq. 41).

which is the mean firing rate of the neuron - a simply measurable quantity.

Second, how would $H_{\rm int}(f)$ change if T_* is varied? Since $H_{\rm int}(f)$ is directly measurable only through $S_Y(f)$ (Eq. 34), we consider $S_Y(f)$ instead. From Eq. 57 it is clear that if $S_Y(f) \sim f^{-\alpha}$ approximately at low frequencies then the exponent α should not depend much on any external parameter (assuming $0 < p_* < 1$). This was observed experimentally when the stimulation rate (T_*^{-1}) was varied, as can be seen in Fig. 1G in [13].

4 Discussion

4.1 Generating $f^{-\alpha}$ PSD.

In this work we aim to explain biophysically the phenomenon of $f^{-\alpha}$ behavior in the response of isolated neurons, and explore its implications on the input-ouput relation of the neuron. We do this under a regime of sparse stimulation (Fig. 1), and in the biophysical framework of stochastic conductance-based models (CBMs, Eqs. 2-4). In this setting our analytical results [46] can be used to derive a closed form expression for the Power Spectral Density (PSD, Eq. 8) based on the parameters of the slow kinetics in the CBM. This PSD is affected by the closed-loop interaction - the slow dynamics affect the AP response, which, in turn, feeds back and affects the kinetics of the slow processes (section 2.3.2). Moreover, the contribution of each slow process to the PSD can be exactly quantified (section 2.3.3), as we demonstrate using a simple model (section 2.3.4).

These mathematical results expose the large parameter degeneracy of CBMs [28, 46], *i.e.*, that many "different" models will quantitatively produce the same behavior. Due the

the degeneracy of CBMs, we first aimed to derive rather general sufficient conditions for the generation of $f^{-\alpha}$ noise in a CBM (section 3.2.1). These conditions indicate which types of CBMs can generate the observed behavior. We show that, in order to generate $f^{-\alpha}$ behavior, neurons should have intrinsic fluctuations (*e.g.* due to ion channel noise), and have a number of slow processes with a large range of timescales, "covering" the entire range over which $f^{-\alpha}$ statistics is observed. Furthermore, the parameters of these processes must be scaled in a certain way in order to generate $f^{-\alpha}$ noise with a specific α (Eq. 24).

We implement these constraints in a minimal CBM (section 3.2.2), in which the slow processes are uncoupled, except through the voltage, as in [48]. Initially, we find that the specific scaling relation can be achieved either by scaling the (1) "magnitude" or (2) the ion channel number - so slower processes will be either (1) "stronger" or (2) "more noisy". However, the "feedback" effect in the model (the slow process being affected by the APs) prevents $f^{-\alpha}$ statistics from being generated in case (1). In contrast, option (2) can robustly generate the observed $f^{-\alpha}$ statistics in the neuronal response for any $0 < \alpha < 2$ (Eq. 28 and Fig. 6).

Naturally, outside of the framework of CBMs (Eqs. 2-4) long term correlations may be modeled differently, since there are numerous distinct ways to generate power law distributions [32]. For example, as numerically demonstrated in [13], $1/f$ statistics in neuronal firing patterns can be generated by assuming global (cooperative) interactions between ion channels (*i.e.*, not through the voltage). Biophysically, the significance of interactions between ion channels is still not clear ([31] and Brief Communications arising), but other cellular processes that might affect excitability on slower timescales clearly exhibit interactions (*e.g.*, gene regulation networks [7]). Mathematically, such interactions render the slow dynamics (Eq. 4) non-linear at constant voltage [15]. It would be interesting to generalize the theory we presented here in order to understand how to tune the PSD in such a non-linear setting, since this has the potential to further reduce the number of parameters and model complexity.

4.2 Biophysical implementation.

We examine our theoretical predictions numerically. We do this using a stochastic Hodgkin Huxley type model with slow sodium inactivation that was previously fitted to the basic experimental results [48]. We extend this model to include four additional slow processes, which resemble slow sodium inactivation (section C.2). The only difference is that each process is slower than the previous one, and has a lower number of ion channels, according to the specific scaling relation that was derived. The resulting model indeed generates $f^{-\alpha}$ noise, and is demonstrated numerically (Fig. 3) to fit the experimental results of [11]. This is the first time, to our knowledge, that a cortical neuron model (either biophysical or phenomenological) reproduces experimental results over such long timescales. Notably, without the analytical results, it would be hard to tune the parameters of a biophysical neuron, due to the large number of unknown parameters.

Previous works [24, 45] demonstrated numerically that, even with constant current stimulation, incorporating slow processes into an excitable cell model can generate $f^{-\alpha}$ in its response. In [24] a HH model was extended to include multiple slow processes with scaled rates in the potassium channel produced $f^{-\alpha}$ firing rate response. Their model produced an exponent of $\alpha \approx 0.5$, replicating experiments measurements from

the auditory nerves. Another work [45], aiming to reproduce the activity of heart cells, produced long term correlations with $\alpha \approx 1.6 - 2$ using a reflected diffusion process.

The identity of the specific slow processes involved in generating $f^{-\alpha}$ remains a mystery at this point, since there are many possible mechanisms which can modulate the excitability of the cell in such long timescales. For example, ion channel numbers, conductances and kinetics are constantly being regulated and may change over time (*e.g.*, [23, 49]). Also, the ionic concentrations in the cell depend on the activity of the ionic pumps, which can be affected by metabolism [43]. Finally, the spike initiation region can significantly shift its location with time (*e.g.*, 17 μm distally during 48 hours of high activity [18]), and so can cellular neurites [36, 33]. Only after such slow processes are quantitatively characterized, we can determine their effect on the neuron's excitability at long timescales.

4.3 The input-output relation.

The linearized input-output relation of the fitted CBM was derived using the methods described in [46]. This linearized relation decomposes the contributions of external inputs and internal fluctuations to the response of the neuron. This decomposition (Eq. 31) shows that even though the neuron can "remember" its intrinsic fluctuations over timescales of days, its memory of past pulse inputs can be limited to a shorter timescale of $\sim 10^2$ sec (Fig. 4). Notably, the neuron has this limited memory for such inputs even though processes on much slower timescales exist in the model.

In the introduction we mentioned previous works [27, 26, 39] which also described the temporal integration in the neuron using power-law filters, although in a rather different (non-sparse) stimulation regime. Our fitted model indicates that similar power-law integration still occurs at very long timescales. However, it is not the input that is being integrated, but the internal fluctuations in the neuron, and this is what drives the $f^{-\alpha}$ statistics measured by [11]. Also, as in [27, 26, 39], the neuronal response in our model is indeed affected by the last 10 sec of its external inputs. However, our model suggests the response will not be significantly affected by spike perturbations in its input that occurred more than 10^2 sec ago.

Qualitatively, this specific timescale of the input memory stems from the "fastest slow negative feedback process" in the model (in this specific model, slow sodium inactivation). This process responds to perturbations in the input which change the firing rate much more quickly then all the other slow processes. Its response to perturbation brings the firing rate back to its steady state, before slower processes even register that the firing rate has changed. Therefore, effectively, these slower processes do not store much information about input perturbations. We suggest experiments to test input memory directly, by using $f^{-\alpha}$ stimulation (Fig. 5A), "sum of sines" stimulation (Fig. 5B) and a variation of the mean stimulation rate (Eq. 42 and Fig. 7).

Appendix

A Detailed derivations

A.1 Derivation of Eqs. 13-14

Recall Eq. 11.

$$S_Y^o(f) \triangleq T_* \sigma_e^2 + \mathbf{w}^\top \mathbf{H}_o(-f) \mathbf{D}_* \mathbf{H}_o^\top(f) \mathbf{w}.$$

Suppose that $\mathbf{A}_*$ is diagonalizable, so that we can write $\mathbf{A}_* = \mathbf{U}\tilde{\mathbf{A}}\mathbf{V}$, where $\mathbf{U} = \mathbf{V}^{-1}$ and $\tilde{\mathbf{A}}$ is some diagonal matrix. In that case

$$\begin{aligned}
& \mathbf{w}^\top \mathbf{H}_o(-f) \mathbf{D}_* \mathbf{H}_o^\top(f) \mathbf{w} \\
= \; & \mathbf{w}^\top (-2\pi f i \mathbf{I} - \mathbf{A}_*)^{-1} \mathbf{D}_* \left(2\pi f i \mathbf{I} - \mathbf{A}_*^\top\right)^{-1} \mathbf{w} \\
= \; & \mathbf{w}^\top \left(-2\pi f i \mathbf{I} - \mathbf{U}\tilde{\mathbf{A}}\mathbf{V}\right)^{-1} \mathbf{D}_* \left(2\pi f i \mathbf{I} - \mathbf{V}^\top \tilde{\mathbf{A}} \mathbf{U}^\top\right)^{-1} \mathbf{w} \\
= \; & \mathbf{w}^\top \mathbf{V}^{-1} \left(-2\pi f i \mathbf{I} - \tilde{\mathbf{A}}\right)^{-1} \mathbf{U}^{-1} \mathbf{D}_* \left(\mathbf{U}^{-1}\right)^\top \left(2\pi f i \mathbf{I} - \tilde{\mathbf{A}}\right)^{-1} \left(\mathbf{V}^{-1}\right)^\top \mathbf{w} \\
= \; & \tilde{\mathbf{w}}^\top \left(-2\pi f i \mathbf{I} - \tilde{\mathbf{A}}\right)^{-1} \tilde{\mathbf{D}} \left(2\pi f i \mathbf{I} - \tilde{\mathbf{A}}\right)^{-1} \tilde{\mathbf{w}}
\end{aligned}$$

where in the last line we denoted $\tilde{\mathbf{w}} = \left(\mathbf{V}^{-1}\right)^\top \mathbf{w}$ and $\tilde{\mathbf{D}} = \mathbf{U}^{-1}\mathbf{D}_* \left(\mathbf{U}^{-1}\right)^\top$. Denoting $D_{kj} = \left(\tilde{\mathbf{D}}\right)_{kj}$, $A_{kj} = \left(\tilde{\mathbf{A}}\right)_{kj}$, $A_k = A_{kk}$ and $w_k = (\tilde{\mathbf{w}})_k$, and noting that $\tilde{\mathbf{D}}$ is a symmetric matrix (since $\mathbf{D}_*$ is symmetric), the last line can be decomposed into partial fractions in the following way

$$\begin{aligned}
& \tilde{\mathbf{w}}^\top \left(-2\pi f i \mathbf{I} - \tilde{\mathbf{A}}\right)^{-1} \tilde{\mathbf{D}} \left(2\pi f i \mathbf{I} - \tilde{\mathbf{A}}\right)^{-1} \tilde{\mathbf{w}} \\
= \; & \sum_{k,j} \frac{w_k D_{kj} w_j}{(-2\pi f i - A_k)(2\pi f i - A_j)} \\
= \; & -\sum_{k,j} \frac{w_k D_{kj} w_j}{A_k + A_j} \left[\frac{1}{-2\pi f i - A_k} + \frac{1}{2\pi f i - A_j}\right] \\
= \; & \sum_{k,j} \frac{w_k D_{kj} w_j}{A_k + A_j} \left[\frac{1}{2\pi f i + A_k} + \frac{1}{-2\pi f i + A_k}\right] \\
= \; & 2\sum_{k,j} \frac{w_k D_{kj} w_j}{A_k + A_j} \left[\frac{A_k}{(2\pi f)^2 + A_k^2}\right] \\
= \; & \sum_k \left(\sum_j w_k D_{kj} w_j \frac{2A_k}{A_k + A_j}\right) \frac{1}{(2\pi f)^2 + A_k^2}
\end{aligned}$$

which gives Eqs. 13-14.

A.2 Complex poles

Suppose the partial fraction decomposition of $S_Y^o(f)$ (Eq. 13) contains complex poles. Since $S_Y^o(f)$ is real, these poles must appear for complex conjugate pairs λ, $\bar{\lambda}$, with complex conjugate amplitudes, as follows

$$\begin{aligned} & \frac{c}{(2\pi f)^2+\lambda^2}+\frac{\bar{c}}{(2\pi f)^2+\bar{\lambda}^2} \\ = & \frac{c\left((2\pi f)^2+\bar{\lambda}^2\right)+\bar{c}\left((2\pi f)^2+\lambda^2\right)}{\left((2\pi f)^2+\lambda^2\right)\left((2\pi f)^2+\bar{\lambda}^2\right)} \\ = & \frac{(2\pi f)^2(c+\bar{c})+c\bar{\lambda}^2+\bar{c}\lambda^2}{(2\pi f)^4+(2\pi f)^2\left(\lambda^2+\bar{\lambda}^2\right)+|\lambda|^2}. \end{aligned} \tag{43}$$

Denoting $e^{i\theta} \triangleq \lambda/|\lambda|$ and $e^{i\phi} \triangleq c/|c|$ we can write Eq. 43 as

$$\begin{aligned} & 2|c|\frac{(2\pi f)^2\cos(\phi)+|\lambda|^2\cos(\phi+2\theta)}{(2\pi f)^4+2(2\pi f)^2|\lambda|^2\cos(2\theta)+|\lambda|^4} \\ = & \begin{cases} \frac{2|c|\cos(\phi)}{(2\pi f)^2} & , \text{if } 2\pi f \gg |\lambda| \\ \frac{|c|}{|\lambda|^2}\frac{\cos(\phi)+\cos(\phi+2\theta)}{1+\cos(2\theta)} & , \text{if } 2\pi f \sim |\lambda| \\ \frac{2|c|\cos(\phi+2\theta)}{|\lambda|^2} & , \text{if } 2\pi f \ll |\lambda| \end{cases}. \end{aligned} \tag{44}$$

Note that for $2\pi f \sim |\lambda|$, this can go to infinity if $\theta \to \pm\pi/2$. In comparison, for a real pole

$$\frac{c}{(2\pi f)^2+\lambda^2} = \begin{cases} \frac{c}{(2\pi f)^2} & , \text{if } 2\pi f \gg |\lambda| \\ \frac{c}{2|\lambda|^2} & , \text{if } 2\pi f \sim |\lambda| \\ \frac{c}{|\lambda|^2} & , \text{if } 2\pi f \ll |\lambda| \end{cases}.$$

Therefore, the asymptotic behavior is similar, except that for a simple pole there is a different pre-factor in each region.

A.3 Derivation of Eq. 24

From Eq. 22, we have

$$S_Y^o(f) = \int \frac{\rho(\lambda)\,d\lambda}{(2\pi f)^2+\lambda^2}.$$

We define $\tilde{\rho}(\lambda) = |\lambda|^{\alpha-1}\rho(\lambda)$ and recall that $\rho(\lambda) = 0$ outside of the range $|\lambda_M| < |\lambda| < |\lambda_{L+1}|$. We obtain

$$\begin{aligned} S_Y^o(f) &= \int_{\lambda_{L+1}}^{\lambda_M} \frac{(-\lambda)^{1-\alpha}\tilde{\rho}(\lambda)}{(2\pi f)^2+\lambda^2}\,d\lambda \\ &\overset{u=\frac{-\lambda}{2\pi f}}{=} (2\pi f)^{-\alpha}\int_{-\lambda_M/2\pi f}^{-\lambda_{L+1}/2\pi f} \frac{u^{1-\alpha}\tilde{\rho}(-2\pi f u)}{1+u^2}\,du \\ &\to (2\pi f)^{-\alpha}\int_0^{\infty} \frac{u^{1-\alpha}\tilde{\rho}(-2\pi f u)}{1+u^2}\,du \end{aligned} \tag{45}$$

where we assumed in the last line that$|\lambda_{L+1}| \gg 2\pi f \gg |\lambda_M|$ and recall that $0 < \alpha < 2$ (note that if $\alpha < 0$ or $\alpha > 2$, the last integral will diverge). Therefore, clearly

$$S_Y^o(f) \propto f^{-\alpha} \tag{46}$$

in that range if $\tilde{\rho}(\lambda)$ is constant.

However, is this also necessary condition? In order that Eq. 46 would remain true we must have

$$\int_0^{\infty} \frac{u^{1-\alpha}\tilde{\rho}(-2\pi f u)}{1+u^2}\,du = C, \tag{47}$$

where C is some finite constant. To show that this must imply that $\tilde{\rho}(\lambda)$ is constant we define $x = -\ln(2\pi f)$, and $\hat{\rho}(-\ln(-x)) \triangleq \tilde{\rho}(x)$. Eq. 47 then becomes

$$\int_0^{\infty} \frac{u^{1-\alpha}\hat{\rho}(x-\ln u)}{1+u^2}\,du = C\,.$$

Changing variables to $v = \ln u$ (so $u = e^v$ and $du = e^v dv$) we obtain

$$\int_{-\infty}^{\infty} \frac{e^{-\alpha v}\hat{\rho}(x-v)}{1+e^{-2v}}\,dv = (\psi * \hat{\rho})(x) = C \tag{48}$$

with $*$ denoting the convolution operation and

$$\psi(x) \triangleq \frac{e^{-\alpha v}}{1+e^{-2v}}\,.$$

Assuming that the (generalized) Fourier transform of ρ,

$$\varrho(\omega) \triangleq \int_{-\infty}^{\infty} \hat{\rho}(x)\,e^{-i\omega x}dx\,,$$

exists, we take the Fourier transform of Eq. 48, and obtain

$$\Psi(\omega)\,\varrho(\omega) = 2\pi C\delta(\omega) \tag{49}$$

where $\delta(\omega)$ is Dirac's delta function, and

$$\Psi(\omega) \triangleq \int_{-\infty}^{\infty} \psi(x)\,e^{-i\omega x}dx = \frac{\pi}{2\sin(\pi(\alpha+i\omega)/2)}\,. \tag{50}$$

Therefore, From Eqs. 49-50, we obtain

$$\varrho(\omega) = \frac{C\delta(\omega)}{\Psi(0)} = 4C\sin(\pi\alpha/2)\,\delta(\omega)$$

and so

$$\hat{\rho}(x) = 2\pi^{-1}C\sin(\pi\alpha/2),$$

a constant. Therefore, $\tilde{\rho}(x)$ is also a constant, which is what we wanted to prove.

To summarize, we find that

$$S_Y^o(f) = Cf^{-\alpha}. \tag{51}$$

if and only if

$$\rho(\lambda) = 2\pi^{-1}C\sin(\pi\alpha/2)\,|\lambda|^{1-\alpha}. \tag{52}$$

A.4 Derivation of Eq. 28 and related matters

In the diagonal model presented in section 3.2.2

$$S_Y^o(f) = T_*\sigma_e^2 + \sum_{k=1}^{M}\frac{c_k}{(2\pi f)^2 + \lambda_k^2}, \tag{53}$$

with $\lambda_k = \lambda_1\epsilon^{k-1}$, and

$$c_k = \frac{w_k^2}{N_{s,k}}\frac{\gamma_{*,k}\delta_{*,k}}{\gamma_{*,k}+\delta_{*,k}} \tag{54}$$

where $w_k = w_1\epsilon^{-\mu(k-1)}$ and $N_{s,k} = N_{s,1}\epsilon^{\nu(k-1)}$. Therefore $c_k = c_1\epsilon^{(1-\eta)(k-1)}$ with $\eta = \nu + 2\mu$, and we can write

$$S_Y^o(f) \;=\; T_*\sigma_e^2 + c_1\sum_{j=0}^{M-1}\frac{\epsilon^{j(1-\eta)}}{(2\pi f)^2 + \lambda_1^2\epsilon^{2j}}.$$

In section A.5, we find that for $|\lambda_M| \ll 2\pi f \ll |\lambda_1|$

$$\sum_{j=0}^{M-1}\frac{\epsilon^{j(1-\eta)}}{(2\pi f)^2 + \lambda_1^2\epsilon^{2j}} \;\approx\; g(\epsilon,\eta)\times\begin{cases}\epsilon^{M(1-\eta)}(2\pi f)^{-2} & ,\text{if } \eta > 1\\ \ln\left(|\lambda_1|\,\epsilon^M/(2\pi f)\right)(2\pi f)^{-2} & ,\text{if } \eta = 1\\ \lambda_1^{-2}\left(\frac{2\pi f}{|\lambda_1|}\right)^{-(1+\eta)} & ,\text{if } 1 > \eta > -1\\ \lambda_1^{-2}\ln(-2\pi f/\lambda_1) & ,\text{if } \eta = -1\\ \lambda_1^{-2} & ,\text{if } \eta < -1\end{cases} \tag{55}$$

where $g(\epsilon,\eta)$ is some proportionality constant that depends only on ϵ and η. This approximation immediately gives us $S_Y^o(f)$. It is accurate both in the limit that the poles are sparse ($\epsilon \to 0$) and in the limit that the poles are dense ($\epsilon \to 1^-$).

Next, we note that $a_k = a_1\epsilon^{k-1}$ with $a_1 = \tau_{\mathrm{AP}}\left(\gamma_{*,1}\left(\delta_{+,1}-\delta_{-,1}\right) - \left(\gamma_{+,1}-\gamma_{-,1}\right)\delta_{*,1}\right)/\left(\gamma_{*,1}+\delta_{*,1}\right)$. Applying these substitutions to Eq. 15, we obtain

$$\begin{aligned}\kappa(f) &= 1 - T_*^{-1} w_1 a_1 \sum_{j=0}^{M-1} \frac{\epsilon^{(1-\mu)j}}{2\pi f i - |\lambda_1| \epsilon^j} \\ &= 1 + T_*^{-1} w_1 a_1 \sum_{j=0}^{M-1} \frac{\epsilon^{(1-\mu)j} \left(2\pi f i + \lambda_1 \epsilon^j\right)}{(2\pi f)^2 + \left(\lambda_1 \epsilon^j\right)^2}.\end{aligned}$$

Therefore

$$\begin{aligned}\frac{\kappa(f) - 1}{T_*^{-1} w_1 a_1 \lambda_1} &= \frac{2\pi f}{\lambda_1} i \cdot g(\epsilon, \mu) \times \begin{cases} \epsilon^{M(1-\mu)} (2\pi f)^{-2} & , \text{if } \mu > 1 \\ \ln\left(|\lambda_1| \epsilon^M / (2\pi f)\right) (2\pi f)^{-2} & , \text{if } \mu = 1 \\ \lambda_1^{-2} \left(\frac{2\pi f}{|\lambda_1|}\right)^{-(1+\mu)} & , \text{if } 1 > \mu > -1 \\ \lambda_1^{-2} \ln(2\pi f / |\lambda_1|) & , \text{if } \mu = -1 \\ \lambda_1^{-2} & , \text{if } \mu < -1 \end{cases} \\ &+ g(\epsilon, \mu - 1) \times \begin{cases} \epsilon^{M(2-\mu)} (2\pi f)^{-2} & , \text{if } \mu > 2 \\ \ln\left(|\lambda_1| \epsilon^M / (2\pi f)\right) (2\pi f)^{-2} & , \text{if } \mu = 2 \\ \lambda_1^{-2} \left(\frac{2\pi f}{|\lambda_1|}\right)^{-\mu} & , \text{if } 2 > \mu > 0 \\ \lambda_1^{-2} \ln(2\pi f / |\lambda_1|) & , \text{if } \mu = 0 \\ \lambda_1^{-2} & , \text{if } \mu < 0 \end{cases} \\ &= \begin{cases} g(\epsilon, \mu - 1) \epsilon^{M(2-\mu)} \left(\frac{2\pi f}{|\lambda_1|}\right)^{-2} & , \text{if } \mu > 2 \\ g(\epsilon, \mu - 1) \ln\left(|\lambda_1| \epsilon^M / (2\pi f)\right) \left(\frac{2\pi f}{|\lambda_1|}\right)^{-2} & , \text{if } \mu = 2 \\ g(\epsilon, \mu - 1) \left(\frac{2\pi f}{|\lambda_1|}\right)^{-\mu} & , \text{if } 2 > \mu \geq 1 \\ (i g(\epsilon, \mu) + g(\epsilon, \mu - 1)) \left(\frac{2\pi f}{|\lambda_1|}\right)^{-\mu} & , \text{if } 1 > \mu > 0 \\ g(\epsilon, \mu - 1) \ln(2\pi f / |\lambda_1|) & , \text{if } \mu = 0 \\ g(\epsilon, \mu - 1) & , \text{if } \mu < 0 \end{cases}\end{aligned}$$

where we used the fact that $2\pi f \ll |\lambda_1|$. Now, if the constant 1 is negligible, then we have

$$|\kappa(f)|^{-2} \approx T_*^2 w_1^{-2} a_1^{-2} \lambda_1^2 \times \begin{cases} g^{-2}(\epsilon, \mu - 1) \epsilon^{-2M(2-\mu)} \left(\frac{2\pi f}{|\lambda_1|}\right)^4 & , \text{if } \mu > 2 \\ g^{-2}(\epsilon, \mu - 1) \left(\ln\left(|\lambda_1| \epsilon^M / (2\pi f)\right)\right)^{-2} \left(\frac{2\pi f}{|\lambda_1|}\right)^4 & , \text{if } \mu = 2 \\ g^{-2}(\epsilon, \mu - 1) \left(\frac{2\pi f}{|\lambda_1|}\right)^{2\mu} & , \text{if } 2 > \mu \geq 1 \\ \left(g^2(\epsilon, \mu) + g^2(\epsilon, \mu - 1)\right)^{-1} \left(\frac{2\pi f}{|\lambda_1|}\right)^{2\mu} & , \text{if } 1 > \mu > 0 \\ g^{-2}(\epsilon, \mu - 1) (\ln(2\pi f / |\lambda_1|))^{-2} & , \text{if } \mu = 0 \\ g^{-2}(\epsilon, \mu - 1) & , \text{if } \mu < 0 \end{cases} \quad (36)$$

Therefore, since $S_Y(f) = S_Y^o(f) |\kappa(f)|^{-2}$, we have (assuming $\sigma_e^2 T_*$ is negligible), for

$\mu = 0$

$$S_Y(f) \approx \frac{g^{-2}(\epsilon,-1)\, g(\epsilon,\eta)\, T_*^2 c_1}{w_1^2 a_1^2 \ln^2(2\pi f/|\lambda_1|)} \times \begin{cases} \epsilon^{M(1-\eta)} \left(\frac{2\pi f}{|\lambda_1|}\right)^{-2} & ,\text{if } \eta > 1 \\ \ln\left(|\lambda_1|\,\epsilon^M/(2\pi f)\right) \left(\frac{2\pi f}{|\lambda_1|}\right)^{-2} & ,\text{if } \eta = 1 \\ \left(\frac{2\pi f}{|\lambda_1|}\right)^{-(1+\eta)} & ,\text{if } 1 > \eta > -1 \\ \ln\left(\frac{2\pi f}{|\lambda_1|}\right) & ,\text{if } \eta = -1 \\ 1 & ,\text{if } \eta < -1 \end{cases} , \tag{57}$$

This approximation captures well the asymptotic behavior of $S_Y(f)$ (Eq. 8) for the HHMS model with $|\lambda_M| \ll 2\pi f \ll |\lambda_1|$, as can be seen in Fig. 6 for various values of η. Note that from Eq. 54 $c_1 \propto w_1^2/N_{s,1}$. Therefore: (1) the parameter w_1 has effectively been canceled out from the expression and does not affect $S_Y(f)$ in this range, (2) $S_Y(f) \propto N_{s,1}^{-1}$.

For $\mu > 0$, we recall that $\eta = \nu + 2\mu$, and note that in the ("relevant") range $-1 < \eta < 1$, due to the effects of feedback (Eq. 56),

$$S_Y(f) = S_Y^o(f)\,|\kappa(f)|^{-2} \propto \begin{cases} f^{-(1+\nu+2\mu)} & ,\mu < 0 \\ f^{-(1+\nu)} & ,2 > \mu > 0 \\ f^{-(1+\nu+2\mu-4)} & ,\mu > 2 \end{cases}$$

so the contribution of μ, the scaling in $\mathbf{w}$, can either decrease the exponent of $S_Y(f)$ (if $\mu < 0$), not change it (if $2 > \mu > 0$) or increase it only if ν is already quite negative ($\nu < -2$). Therefore, ν does not really "help" in increasing the exponent of $S_Y(f)$. If, for example, $\nu = 0$, then we can have $S_Y(f) \propto f^{-\alpha}$ with $\alpha \leq 1$ (which is lower than the observed value of $\alpha \approx 1.4$). Therefore, the "simplest" choice to generate $S_Y(f) \propto f^{-\alpha}$ would be $\mu = 0$ and $\nu = \eta$ with η slightly higher than $\alpha - 1$ (due to the logarithmic correction in Eq. 57).

A.5 Derivation of Eq. 55

We wish to calculate the sum

$$\sum_{j=0}^{M-1} \frac{\epsilon^{j(1-\eta)}}{(2\pi f)^2 + \lambda_1^2 \epsilon^{2j}} .$$

assuming that

$$|\lambda_1|\,\epsilon^{M-1} \ll 2\pi f \ll |\lambda_1| . \tag{58}$$

We shall do this in two opposing limits - when the poles are sparse, and when they are dense.

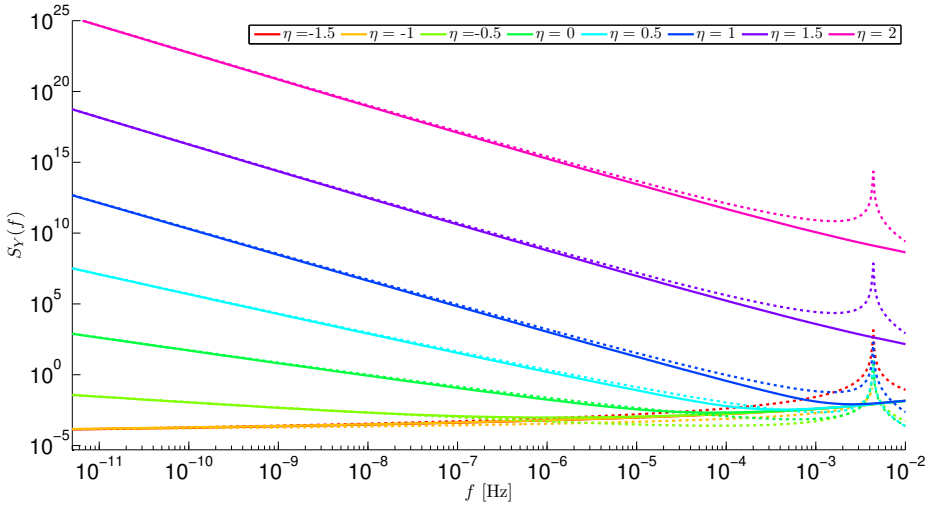

Figure 6: Analytic expression $S_Y(f)$ (full line, Eq. 8) for the HHMS model and its asymptotic approximation (dotted line, Eq. 57, with fitted pre-factors), for different values of η, with $I = 7.5\mu A$, $M = 20$ and $\epsilon = 0.2$. Note that the slopes match the analytical approximation well and increase with η when $\eta \in [-1, 1]$. However, near $f \sim f_{\max}$ the asymptotic approximation becomes inaccurate (and even diverges, due to the logarithmic factor).

A.5.1 Sparse poles

First, we assume the poles are sparse (*i.e.*, well separated, so $\epsilon \ll 1$). We denote $j_* \triangleq \lceil \ln(2\pi f/|\lambda_1|)/\ln\epsilon \rceil$ (where $\lceil\cdot\rceil$ denotes the upper integer values), so

$$
\begin{aligned}
\sum_{j=0}^{M-1} \frac{\epsilon^{j(1-\eta)}}{(2\pi f)^2 + \lambda_1^2 \epsilon^{2j}} &\approx \sum_{j=j_*}^{M-1} \frac{\epsilon^{j(1-\eta)}}{(2\pi f)^2} + \sum_{j=0}^{j_*-1} \frac{\epsilon^{j(1-\eta)}}{\lambda_1^2 \epsilon^{2j}} \\
&= (2\pi f)^{-2} \sum_{j=j_*}^{M-1} \epsilon^{j(1-\eta)} + \lambda_1^{-2} \sum_{j=0}^{j_*-1} \epsilon^{-j(1+\eta)} \\
&\overset{\forall \eta \neq \pm 1}{=} (2\pi f)^{-2} \frac{\epsilon^{j_*(1-\eta)} - \epsilon^{M(1-\eta)}}{1-\epsilon^{(1-\eta)}} + \lambda_1^{-2} \frac{1-\epsilon^{-j_*(1+\eta)}}{1-\epsilon^{-(1+\eta)}} \\
&\approx (2\pi f)^{-2} \frac{(-2\pi f/|\lambda_1|)^{(1-\eta)} - \epsilon^{M(1-\eta)}}{1-\epsilon^{(1-\eta)}} + \lambda_1^{-2} \frac{1-(2\pi f/|\lambda_1|)^{-(1+\eta)}}{1-\epsilon^{-(1+\eta)}} \\
&\approx \begin{cases} (2\pi f)^{-2} \frac{\epsilon^{M(1-\eta)}}{\epsilon^{(1-\eta)}-1} & , \text{if } \eta > 1 \\ \lambda_1^{-2} \left(\frac{2\pi}{|\lambda_1|}\right)^{-(1+\eta)} \left(\frac{1}{1-\epsilon^{(1-\eta)}} - \frac{1}{1-\epsilon^{-(1+\eta)}}\right) \cdot f^{-(1+\eta)} & , \text{if } 1 > \eta > -1 \\ \frac{\lambda_1^{-2}}{1-\epsilon^{-(1+\eta)}} & , \text{if } \eta < -1 \end{cases}
\end{aligned}
$$

where in the last line we used the assumption in Eq. 58. Next, for $\eta = 1$,

$$\begin{aligned}
\sum_{j=0}^{M-1} \frac{1}{(2\pi f)^2 + \lambda_1^2 \epsilon^{2j}} &\approx (2\pi f)^{-2} \sum_{j=j_*}^{M-1} 1 + \lambda_1^{-2} \sum_{j=0}^{j_*-1} \epsilon^{-2j} \\
&= (2\pi f)^{-2} (M - j_*) + \frac{\lambda_1^{-2} - (2\pi f)^{-2}}{1 - \epsilon^{-2}} \\
&\approx (2\pi f)^{-2} \ln\left(|\lambda_1| \epsilon^M / (2\pi f)\right) / \ln \epsilon \,,
\end{aligned}$$

where in the last line we used the assumption in Eq. 58. Next, for $\eta = -1$,

$$\begin{aligned}
\sum_{j=0}^{M-1} \frac{\epsilon^{2j}}{(2\pi f)^2 + \lambda_1^2 \epsilon^{2j}} &\approx (2\pi f)^{-2} \sum_{j=j_*}^{M-1} \epsilon^{-2j} + \lambda_1^{-2} \sum_{j=0}^{j_*-1} 1 \\
&= (2\pi f)^{-2} \frac{(2\pi f / |\lambda_1|)^2 - \epsilon^{2M}}{1 - \epsilon^2} + \lambda_1^{-2} j_* \\
&\approx \lambda_1^{-2} \ln(2\pi f / |\lambda_1|) / \ln \epsilon
\end{aligned}$$

A.5.2 Dense poles

Next, we assume the poles are dense (*i.e.*, very close to each other, so $1 - \epsilon \ll 1$). In this case, we denote, $\lambda_j = |\lambda_1| \epsilon^j$, $d\lambda_j = \lambda_{j-1} - \lambda_j = (1 - \epsilon) |\lambda_1| \epsilon^{j-1} = \left(\epsilon^{-1} - 1\right) \lambda_j$, so

$$
\begin{aligned}
& (|\lambda_1|)^{1-\eta}\left(\epsilon^{-1}-1\right)\sum_{j=0}^{M-1}\frac{\epsilon^{j(1-\eta)}}{(2\pi f)^2+\lambda_1^2\epsilon^{2j}} \\
= & \sum_{j=0}^{M-1}\frac{\lambda_j^{-\eta}d\lambda_j}{(2\pi f)^2+\lambda_j^2} \\
\approx & \int_{|\lambda_1|\epsilon^{M-1}}^{|\lambda_1|}\frac{\lambda^{-\eta}d\lambda}{(2\pi f)^2+\lambda^2} \\
= & (2\pi f)^{-\eta-1}\int_{|\lambda_1|\epsilon^{M-1}}^{|\lambda_1|}\frac{(\lambda/2\pi f)^{-\eta}\,d\,(\lambda/2\pi f)}{1+(\lambda/2\pi f)^2} \\
= & (2\pi f)^{-\eta-1}\int_{|\lambda_1|\epsilon^{M-1}/2\pi f}^{|\lambda_1|/2\pi f}\frac{x^{-\eta}dx}{1+x^2} \\
\approx & (2\pi f)^{-\eta-1}\cdot\begin{cases}\int_{|\lambda_1|\epsilon^{M-1}/2\pi f}^{\infty}\frac{x^{-\eta}dx}{1+x^2} & ,\text{if } \eta\geq 1\\ \int_0^{\infty}\frac{x^{-\eta}dx}{1+x^2} & ,\text{if } 1>\eta>-1\\ \int_0^{|\lambda_1|/2\pi f}\frac{x^{-\eta}dx}{1+x^2} & ,\text{if } \eta\leq -1\end{cases} \\
\approx & (2\pi f)^{-\eta-1}\cdot\begin{cases}\left(|\lambda_1|\,\epsilon^{M-1}/2\pi f\right)^{-\eta+1}/(\eta-1) & ,\text{if } \eta>1\\ \ln\left(2\pi f/|\lambda_1|\,\epsilon^{M-1}\right) & ,\text{if } \eta=1\\ \int_0^{\infty}\frac{x^{-\eta}dx}{1+x^2} & ,\text{if } 1>\eta>-1\\ \ln\left(|\lambda_1|/2\pi f\right) & ,\text{if } \eta=-1\\ \left(|\lambda_1|/2\pi f\right)^{-\eta-1}/(-\eta-1) & ,\text{if } \eta<-1\end{cases} \\
= & \begin{cases}\frac{1}{\eta-1}\left(|\lambda_1|\,\epsilon^{M-1}\right)^{-\eta+1}\cdot(2\pi f)^{-2} & ,\text{if } \eta>1\\ \ln\left(2\pi f/|\lambda_1|\,\epsilon^{M-1}\right)\cdot(2\pi f)^{-2} & ,\text{if } \eta=1\\ \frac{\pi}{2\cos(\pi\eta/2)}\cdot(2\pi f)^{-\eta-1} & ,\text{if } 1>\eta>-1\\ \ln\left(|\lambda_1|/2\pi f\right) & ,\text{if } \eta=-1\\ \frac{1}{-\eta-1}|\lambda_1|^{-\eta-1} & ,\text{if } \eta<-1\end{cases}.
\end{aligned}
$$

A.5.3 Summary

In the dense limit

$$
\sum_{j=0}^{M-1}\frac{\epsilon^{j(1-\eta)}}{(2\pi f)^2+\lambda_1^2\epsilon^{2j}}\approx\left(\epsilon^{-1}-1\right)^{-1}\begin{cases}\frac{1}{\eta-1}\left(\epsilon^{M-1}\right)^{-\eta+1}\cdot(2\pi f)^{-2} & ,\text{if } \eta>1\\ \ln\left(2\pi f/|\lambda_1|\,\epsilon^{M-1}\right)\cdot(2\pi f)^{-2} & ,\text{if } \eta=1\\ \frac{\pi\lambda_1^{-2}}{2\cos(\pi\eta/2)}\cdot\left(\frac{2\pi f}{|\lambda_1|}\right)^{-(\eta+1)} & ,\text{if } 1>\eta>-1\\ \lambda_1^{-2}\ln\left(|\lambda_1|/2\pi f\right) & ,\text{if } \eta=-1\\ \frac{1}{-\eta-1}\lambda_1^{-2} & ,\text{if } \eta<-1\end{cases}.
$$

In the sparse pole limit

$$\sum_{j=0}^{M-1}\frac{\epsilon^{j(1-\eta)}}{\left(2\pi f\right)^{2}+\lambda_{1}^{2}\epsilon^{2j}} \approx \begin{cases} \frac{\epsilon^{M(1-\eta)}}{\epsilon^{(1-\eta)}-1}\left(2\pi f\right)^{-2} & ,\text{if } \eta>1 \\ \left[\ln\left(\left|\lambda_{1}\right|\epsilon^{M}/\left(2\pi f\right)\right)/\ln\epsilon\right]\left(2\pi f\right)^{-2} & ,\text{if } \eta=1 \\ \lambda_{1}^{-2}\left(\frac{1}{1-\epsilon^{(1-\eta)}}-\frac{1}{1-\epsilon^{-(1+\eta)}}\right)\cdot\left(\frac{2\pi f}{\left|\lambda_{1}\right|}\right)^{-(1+\eta)} & ,\text{if } 1>\eta>-1 \\ \lambda_{1}^{-2}\ln\left(2\pi f/\left|\lambda_{1}\right|\right)/\ln\epsilon & ,\text{if } \eta=-1 \\ \frac{\lambda_{1}^{-2}}{1-\epsilon^{-(1+\eta)}} & ,\text{if } \eta<-1 \end{cases}$$

So, in general, assuming some continuity between both limits

$$\sum_{j=0}^{M-1}\frac{\epsilon^{j(1-\eta)}}{\left(2\pi f\right)^{2}+\lambda_{1}^{2}\epsilon^{2j}} \approx c\left(\epsilon,\eta\right)\cdot\begin{cases} \epsilon^{M(1-\eta)}\left(2\pi f\right)^{-2} & ,\text{if } \eta>1 \\ \ln\left(\left|\lambda_{1}\right|\epsilon^{M}/\left(2\pi f\right)\right)\left(2\pi f\right)^{-2} & ,\text{if } \eta=1 \\ \lambda_{1}^{-2}\left(\frac{2\pi f}{\left|\lambda_{1}\right|}\right)^{-(1+\eta)} & ,\text{if } 1>\eta>-1 \\ \lambda_{1}^{-2}\ln\left(2\pi f/\left|\lambda_{1}\right|\right) & ,\text{if } \eta=-1 \\ \lambda_{1}^{-2} & ,\text{if } \eta<-1 \end{cases} \tag{59}$$

where $c\left(\epsilon,\eta\right)$ is some proportionality constant that depends only on ϵ and η. Note that in both cases $c\left(\epsilon,\eta\right)$ diverges when $\eta\to\pm1,\infty$ or when $\epsilon\to1$.

A.6 Derivation of Eq. 39

From Eq. 35, using similar notation and analysis as in the previous section, we write

$$H^{\text{ext}}\left(f\right)=H^{\text{ext}}\left(f\right)/\kappa\left(f\right)$$

with

$$H^{\text{ext}}\left(f\right) \triangleq T_{*}^{-1}\mathbf{w}^{\top}\left(2\pi fi\mathbf{I}-\mathbf{A}_{*}\right)^{-1}\mathbf{d}$$

being the "open loop" version of $H^{\text{ext}}\left(f\right)$ (*i.e.*, if $\boldsymbol{a}$ was zero). For $2\pi f\gg\left|\lambda_{1}\right|$ we have

$$\begin{aligned} \kappa\left(f\right) &= 1+T_{*}^{-1}w_{1}a_{1}\sum_{j=0}^{M-1}\frac{\epsilon^{j}\left(2\pi fi+\left|\lambda_{1}\right|\epsilon^{j}\right)}{\left(2\pi f\right)^{2}+\left(\lambda_{1}\epsilon^{j}\right)^{2}} \\ &\approx 1+\frac{iT_{*}^{-1}w_{1}a_{1}}{2\pi f}\sum_{j=0}^{M-1}\epsilon^{j} \\ &= 1+\frac{iT_{*}^{-1}w_{1}a_{1}}{2\pi f\left(1-\epsilon\right)} \end{aligned}$$

where we assumed $\left(1-\epsilon^{M}\right)\approx1$. Similarly, for $2\pi f\gg\left|\lambda_{1}\right|$,

$$\begin{aligned} H^{\text{ext}}\left(f\right) &= -T_{*}^{-1}w_{1}d_{1}\sum_{j=0}^{M-1}\frac{\epsilon^{j}\left(2\pi fi+\left|\lambda_{1}\right|\epsilon^{j}\right)}{\left(2\pi f\right)^{2}+\left(\lambda_{1}\epsilon^{j}\right)^{2}} \\ &\approx -\frac{iT_{*}^{-1}w_{1}d_{1}}{2\pi f\left(1-\epsilon\right)} \end{aligned}$$

Therefore, for $2\pi f \gg |\lambda_1|$,

$$\begin{aligned} H^{\text{ext}}(f) &= H^{\text{ext}}(f)/\kappa(f) \\ &\approx \frac{T_*^{-1} w_1 d_1 (1-\epsilon)^{-1}}{2\pi f i - T_*^{-1} w_1 a_1 (1-\epsilon)^{-1}}. \end{aligned} \tag{60}$$

For $|\lambda_1|\epsilon^M \ll 2\pi f \ll |\lambda_1|$, using Eq. 56 for $\mu = 0$, we obtain

$$\begin{aligned} \kappa(f) &\approx 1 + T_*^{-1} w_1 a_1 \lambda_1^{-2} \left[i\lambda_1^{-1} g(\epsilon, 0) |\lambda_1| \ln(2\pi f/|\lambda_1|) \, g(\epsilon, -1) \right] \\ &\approx \frac{w_1 a_1 g(\epsilon, -1)}{-T_* \lambda_1} \ln(2\pi f/|\lambda_1|) \end{aligned}$$

and, similarly

$$\begin{aligned} H^{\text{ext}}(f) &\approx -T_*^{-1} w_1 d_1 \lambda_1^{-2} \left[i\lambda_1^{-1} g(\epsilon, 0) |\lambda_1| \ln(2\pi f/|\lambda_1|) \, g(\epsilon, -1) \right] \\ &\approx \frac{w_1 d_1 g(\epsilon, -1)}{T_* \lambda_1} \ln(2\pi f/|\lambda_1|) \end{aligned}$$

so

$$H^{\text{ext}}(f) = H^{\text{ext}}(f)/\kappa(f) = -\frac{d_1}{a_1}.$$

Note that this expression matches with Eq. 60 for $f \to 0$.

A.7 Derivation of Eq. 42

Recall, from Eq. 39, that for $2\pi f \gg (1-\epsilon)^{-1} T_*^{-1} w_1 a$

$$H^{\text{ext}}(f) \approx -\frac{d_1}{a_1}. \tag{61}$$

We can simplify this expression further by substituting the expressions for a_1 and d_1. As noted in [48, , Fig. 4B] (where the $+/-/0$ notation is replaced with $H/M/L$ notation), in the HHS model $\gamma(V)$ has a high voltage threshold $\gamma_+ \gg \max(\gamma_-, \gamma_0)$ and $\delta(V)$ has a rather low voltage threshold, so it is approximately voltage independent, with

$$\delta_+ \approx \delta_- \approx \delta_0 \approx \delta_* \triangleq \delta. \tag{62}$$

Therefore,

$$a_1 = \tau_{\text{AP}} \left(\gamma_* (\delta_+ - \delta_-) - (\gamma_+ - \gamma_-) \delta_* \right) / (\gamma_* + \delta_*) \approx -(\gamma_+ - \gamma_-) \delta \tau_{\text{AP}} / (\gamma_* + \delta)$$

and

$$d_1 = (\gamma_* \delta_0 - \gamma_0 \delta_*) / (\gamma_* + \delta_*) \approx (\gamma_* - \gamma_0) \delta / (\gamma_* + \delta).$$

Finally, using

$$\gamma_* \triangleq (p_* \gamma_+ + (1-p_*)\gamma_-) \tau_{\text{AP}} T_*^{-1} + \left(1 - \tau_{\text{AP}} T_*^{-1}\right) \gamma_0 \approx p_* \gamma_+ \tau_{\text{AP}} T_*^{-1} + \gamma_0 \tag{63}$$

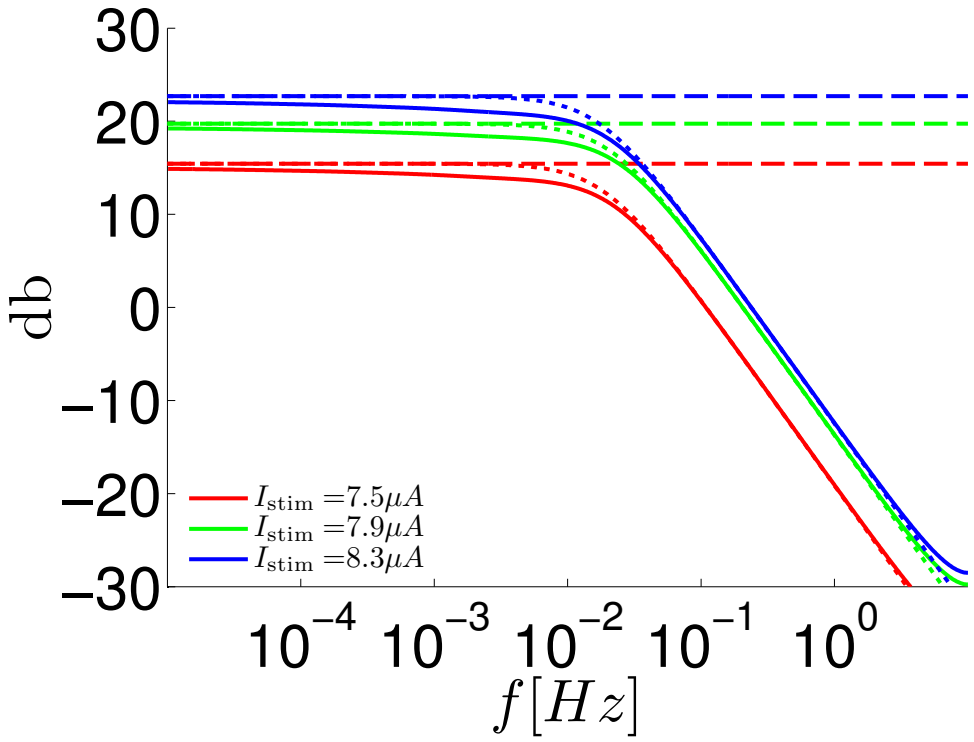

Figure 7: The external input filter $H^{\text{ext}}(f)$ in the HHMS model - comparison of analytical expression (Eq. 35, solid line), asymptotic approximation (Eq. 39, dotted line) and $p_* T_*^{-1} \approx H^{\text{ext}}(0)$ value (Eq. 64, dashed line).

and $\gamma_+ - \gamma_- \approx \gamma_+$, we have, for $|\lambda_1|\,\epsilon^M \ll 2\pi f \ll |\lambda_1|$,

$$-\frac{d_1}{a_1} = \frac{\gamma_* - \gamma_0}{\gamma_+ \tau_{\text{AP}}} \approx p_* T_*^{-1}\,.$$

Therefore, in that range,

$$H^{\text{ext}}(f) \approx -\frac{d_1}{a_1} \approx \frac{p_*}{T_*}\,. \tag{64}$$

Interestingly, we found that $H^{\text{ext}}(0) \approx \bar{f}_{\text{out}} \triangleq p_* T_*^{-1}$, the mean firing rate of the neuron (See Fig. 7).

B Detailed explanation of figures

B.1 Statistical measures in Fig. 3

In Fig. 3 we compare our model to the data using measures that were designed to reveal and estimate "scaling" in empirical signals, as used in [11]. These were applied exactly as in [11]. For completeness, we repeat here the details on how this was done. Further

details on meaning of these measures and the relations among them appear in [5, 25]. The measures used the count process $Z_n(T)$, generated by binning the spikes into N equally sized bins of width T. We further define the empirical average of $Z(T)$

$$\bar{Z}(T) \triangleq N^{-1} \sum_{n=1}^{N} Z_n(T) \tag{65}$$

and the empirical variance

$$\sigma_Z^2(T) \triangleq N^{-1} \sum_{n=1}^{N} \left(Z_n(T) - \bar{Z}(T)\right)^2 \tag{66}$$

If $Z_n(T)$ is a wide-sense stationary signal then for $N \to \infty$ than, from the law of large numbers, Eqs. 65 and 66 should converge to the ensemble averages $\langle Z_n(T) \rangle$ and $\left\langle \hat{Z}_n^2(T) \right\rangle$, respectively.

1. The *rate fluctuations* shows the process

$$\tilde{Z}_n(T) \triangleq Z_n(T) - \bar{Z}(T) \ ,$$

   estimated using bins of different sizes ($T = 10, 30, 100$ and 300 sec) and plotted on a normalized time axis (units in number of bins).

2. The *Coefficient of Variation* (CV) is defined as the ratio of the standard deviation to the mean

$$CV(T) \triangleq \frac{\sigma_Z(T)}{\bar{Z}(T)} \ .$$

3. The *Detrended Fluctuation Analysis* (DFA) [38] was performed as follows. First, $Z_n(T_{\text{bin}})$ was calculated with $T_{\text{bin}} = 1$ sec. Then a piecewise linear curve $U_n(T)$, with segments of length T, was fit to the $Z_n(T_{\text{bin}})$. Then the Root Mean Square Error (RMSE) of the fit is then calculated

$$DFA(T) \triangleq \sqrt{N^{-1} \sum_{n=1}^{N} \left(Z_n(T_{\text{bin}}) - U_n(T)\right)^2}$$

4. The *Fano Factor* (FF) [25] is defined as the variance to mean ratio

$$FF(T) \triangleq \frac{\sigma_Z^2(T)}{\bar{Z}(T)} \ ,$$

5. The *Allan Factor* (AF) [25] is defined as

$$AF(T) \triangleq \frac{N^{-1} \sum_{n=1}^{N} \left(Z_n(T) - Z_{n+1}(T)\right)^2}{2\bar{Z}(T)} \ .$$

6. The firing rate *periodogram,* is an estimate of the power spectral density, as used in [11], namely

$$\tilde{S}_Z(f) \triangleq \frac{T_{\text{bin}}}{N}\left|\sum_{n=1}^{N}\tilde{Z}_n(T_{\text{bin}})\,e^{-2\pi f T_{\text{bin}} n i}\right|^2$$

with $T_{\text{bin}} = 1$ sec. Note that for $N \to \infty$, this should be a "reasonable" [5, 41] estimator for the PSD of $Z_n(T)$

$$S_Z(f) \triangleq T_{\text{bin}}\sum_{k=-\infty}^{\infty}\left\langle \hat{Z}_n(T_{\text{bin}})\,\hat{Z}_{n+k}(T_{\text{bin}})\right\rangle e^{-2\pi f T_{\text{bin}} k i} \tag{67}$$

by the Wiener-Khinchin theorem. It is straightforward to show that for periodical stimulation (*i.e.*, $T_m = T_*$), we have

$$\frac{S_Z(f)}{S_Y(f)} = \begin{cases} W & ,W \le 1 \\ W\frac{\sin^2(\pi f W T_*)}{\sin^2(\pi f T_*)} & ,W \ge 1 \end{cases}$$

where $S_Y(f)$ is given by Eq. 1, we denoted $W \triangleq T_*^{-1}T_{\text{bin}}$, assuming it is an integer. Note that for $f \ll T_{\text{bin}}^{-1}$ this gives

$$\frac{S_Z(f)}{S_Y(f)} \approx \begin{cases} W & ,W \le 1 \\ W^3 & ,W > 1 \end{cases}. \tag{68}$$

B.2 Choosing stimulation type in Fig. 5A

Suppose the stimulation is some random point-process, so $\{T_m\}$ is also a random process. One prediction we could make relates to the shape of $S_{YT}(f)$, which was not measured in [11]. Recall Eqs. 32-33. From Eq. 32, if $S_T(f)$ and $H^{\text{ext}}(f)$ are known then theoretically we can estimate $S_{YT}(f)$. Unfortunately, it is not easy to estimate $S_{YT}(f)$, due to the rather large internal fluctuations in the neuron [46, Fig. 6]. Specifically, suppose $S_{YT}^{\text{est}}(f)$ is our estimator of $S_{YT}(f)$, then the Normalized Mean Square Error (NMSE, see [4, page 321]) is

$$\text{NMSE} \triangleq \frac{\left\langle\left(S_{YT}(f) - S_{YT}^{\text{est}}(f)\right)^2\right\rangle}{\left|S_{YT}(f)\right|^2} \quad \propto \quad \frac{S_T(f)\,S_Y(f)}{\left|S_{YT}(f)\right|^2}.$$

And so, according to Eq. 33,

$$\text{NMSE} \quad \propto \quad 1 + \frac{\left|H_{\text{int}}(f)\right|^2}{\left|H^{\text{ext}}(f)\right|^2 S_T^2(f)}. \tag{69}$$

Therefore, accurate estimation of $S_{YT}(f)$ (or equivalently, identification of $H^{\text{ext}}(f)$) is harder than estimation of $S_Y(f)$ (or equivalently, identification of $H_{\text{int}}(f)$), for which the NMSE $\propto O(1)$ [4].

To overcome the estimation noise problem, we need to increase the "Signal to Noise Ratio" (SNR) in the system by increasing the "signal strength" ($S_T(f)$, the variability in T_m) in comparison with the "noise" (intrinsic fluctuations), so that

$$\left|H^{\text{ext}}(f)\right| S_T(f) \gg \left|H_{\text{int}}(f)\right|$$

in a certain range of f. In that range, we find from Eq. 69 that NMSE $= O(1)$.

As indicated by Fig. 4, we expect that the best SNR would be achieved near 10^{-2}Hz. In order to test our model, we examine experimental data of a neuron under a "$f^{-\alpha}$ stimulation", taken from [12], for which $S_T(f)$ is rather large near 10^{-2}Hz, so $S_{YT}(f)$ can be estimated accurately. In Fig. 5A we see that the estimated $S_{YT}(f)$ is similar to $S_{YT}(f)$ of the fitted model with the same stimulation.

B.3 The math behind Fig. 5B

A useful method for system identification is to excite the system in all its relevant modes [16]. In our case this can be done by a sum of sinusoidal inputs. Specifically, we examine an input

$$\hat{T}_m = \sum_{l=1}^{L} T_{\text{amp}} \sin\left(2\pi f_l T_* m\right) \tag{70}$$

in order to identify $H^{\text{ext}}(f)$, with f_l being some positive "sample" frequencies.

From Eq. 31, the response of the neuron is given by the linear system

$$\hat{Y}(f) = H^{\text{ext}}(f)\hat{T}(f) + H_{\text{int}}(f)z(f) \ .$$

Recall the response of a linear system to a sine input is a sine output, modulated by the magnitude and phase of the linear system at the frequency of the sine [34]. Therefore, in response to the input from Eq. 70,

$$\hat{Y}_m = \sum_{l=1}^{L} T_{\text{amp}} \left|H^{\text{ext}}(f_l)\right| \sin\left(2\pi f_l T_* m + \angle H^{\text{ext}}(f_l)\right) + \mathcal{F}^{-1}\left[H_{\text{int}}(f)z(f)\right] \ .$$

The magnitudes of the sines can be found using a Discrete Fourier Transform (DFT) of $\hat{Y}_m$,

$$\hat{Y}^n(k) \triangleq \sum_{m=0}^{n-1} \hat{Y}_m e^{-2\pi k m i/n}, \qquad k \in \{0,\ldots,n-1\} \ .$$

Since, for large n,

$$\begin{aligned}
\frac{1}{n}\left|\hat{Y}^n(k)\right| &\approx \sum_{l=1}^{L} T_{\text{amp}}\left|H^{\text{ext}}(f_l)\right| \frac{\sin\left(\pi\left(k/n - f_l T_*\right)n\right)}{n\sin\left(\pi\left(k/n - f_l T_*\right)\right)} + \frac{1}{n}\left|H_{\text{int}}(f)z(f)\right|_{f=k/T_* n} \\
&\overset{n\to\infty}{\longrightarrow} \begin{cases} T_{\text{amp}}\left|H^{\text{ext}}(f_l)\right| & \text{, if } k/n \approx f_l T_* \\ 0 & \text{, else} \end{cases},
\end{aligned}$$

where we used the fact that $H_{\text{int}}(f)$ attains its maximal values for $f \to 0$ (where $H_{\text{int}}(f) \sim f^{-\alpha/2}/\ln f$), and, thus, for $k > 0$

$$\frac{1}{n}\left|H_{\text{int}}(f)z(f)\right|_{f=k/T_* n} \le \frac{1}{n}\left|H_{\text{int}}(f)z(f)\right|_{f=1/T_* n} \propto \frac{1}{n}\left|\frac{n^{\alpha/2}}{\ln(1/n)}\right| \overset{n\to\infty}{\longrightarrow} 0$$

for all $\alpha \le 2$. Therefore, if n is large enough, $H^{\text{ext}}(f_l)$ can always be identified as peaks in $\left|\hat{Y}^n(k)\right|/nT_{\text{amp}}$. In Fig. 5B we show that this method seems to work for a simulation of

the fitted HHMS model, with $T_{\text{amp}} = (0.8/L)T_*$ and $L = 9$. An experimental test of this prediction remains to be done, and would verify the linearity of the neuronal response. Note that since $LT_{\text{amp}} = 0.8T_*$, this linear response here cannot be considered simply as a "small signal response".

C Models

C.1 The HHS model

The HHS model [48] combines the Hodgkin-Huxley equations [20] with Slow sodium inactivation [6, 10]. The model equations [48], which employ the uncoupled stochastic noise approximation, are

$$\begin{aligned}
C\dot{V} &= \bar{g}_{Na} s m^3 h \left(E_{Na} - V\right) + \bar{g}_K n^4 \left(E_K - V\right) + \bar{g}_L \left(E_L - V\right) + I\left(t\right) && (71)\\
\dot{m} &= \phi\left[\alpha_m\left(V\right)\left(1-m\right) - \beta_m\left(V\right)m\right] + \sqrt{N^{-1}\phi\left(\alpha_m\left(V\right)\left(1-m\right) + \beta_m\left(V\right)m\right)}\xi_m && (72)\\
\dot{n} &= \phi\left[\alpha_n\left(V\right)\left(1-n\right) - \beta_n\left(V\right)n\right] + \sqrt{N^{-1}\phi\left(\alpha_n\left(V\right)\left(1-n\right) + \beta_n\left(V\right)n\right)}\xi_n && (73)\\
\dot{h} &= \phi\left[\alpha_h\left(V\right)\left(1-h\right) - \beta_h\left(V\right)h\right] + \sqrt{N^{-1}\phi\left(\alpha_h\left(V\right)\left(1-h\right) + \beta_h\left(V\right)h\right)}\xi_h && (74)\\
\dot{s} &= \delta\left(V\right)\left(1-s\right) - \gamma\left(V\right)s + \sqrt{N^{-1}\left(\delta\left(V\right)\left(1-s\right) + \gamma\left(V\right)s\right)}\xi_s && (75)
\end{aligned}$$

where V is the membrane voltage, $I\left(t\right)$ is the input current, r_j are the rapid ion channel "gating variables", s_i are the slow ion channel "gating variables", ξ are white noise processes, $\alpha\left(V\right), \beta\left(V\right), \delta\left(V\right)$, and $\gamma\left(V\right)$ are the voltage dependent kinetic rates of these gating variables, C is the membrane's capacitance, E_K, E_{Na} and E_L are ionic reversal potentials, $\bar{g}_K, \bar{g}_{Na}$ and $\bar{g}_L$ are ionic conductances, and ϕ is an auxiliary dimensionless number, and N are the number of ion channels. Most of the parameters are given their original values (as in [20, 10]):

$$\begin{gathered}
V_{Na} = 50 \text{ mV}, \qquad V_K = -77 \text{ mV}, \qquad V_L = -54 \text{ mV},\\
\bar{g}_{Na} = 120 \ (k\Omega \cdot cm^2)^{-1}, \quad \bar{g}_K = 36 \ (k\Omega \cdot cm^2)^{-1}, \quad g_L = 0.3 \ (k\Omega \cdot cm^2)^{-1},
\end{gathered}$$

$$\begin{aligned}
\alpha_n(V) &= \tfrac{0.01(V+55)}{1-e^{-0.1\cdot(V+55)}} \text{ kHz}, & \beta_n(V) &= 0.125 \cdot e^{-(V+65)/80} \text{ kHz},\\
\alpha_m(V) &= \tfrac{0.1(V+40)}{1-e^{-0.1\cdot(V+40)}} \text{ kHz}, & \beta_m(V) &= 4 \cdot e^{-(V+65)/18} \text{ kHz},\\
\alpha_h(V) &= 0.07 \cdot e^{-(V+65)/20} \text{ kHz}, & \beta_h(V) &= \left(e^{-0.1\cdot(V+35)} + 1\right)^{-1} \text{ kHz},
\end{aligned}$$

where in all the rate functions V is used in units of mV. In order to obtain the specific spike shape and the latency transients observed in cortical neurons, some of the parameters were modified to

$$\begin{aligned}
C_m = 0.5 \ \mu\text{F/cm}^2 \quad &, \quad \phi = 2,\\
\gamma\left(V\right) = 0.51 \cdot (e^{-0.3\cdot(V+17)} + 1)^{-1} \text{ Hz} \quad &, \quad \delta\left(V\right) = 0.05e^{-(V+85)/30} \text{ Hz}\\
N \quad &= \quad 10^6
\end{aligned}$$

These specific choices were fitted to reproduce the basic experimental results of [11] on short timescales (latency transients, firing modes, firing rates and firing patterns) for certain type of neurons (loosely speaking, "non-bursting") [48].

C.2 The HHMS model

In this work we focus on the HHMS model (Hodgkin Huxley model with Many Slow variables). This model is an extension of the HHS model, in which there are many sodium currents, each with different a slow kinetic variable. The equations are identical to the HHS model, except that in Eq. 71 $\bar{g}_{Na}s$ is replaced by $\bar{g}_{Na}M^{-1}\sum_{k=1}^{M}s_k$, where s_1 has the same equation as s in the HHS model, and for $k \geq 2$,

$$\dot{s}_k = \left[\delta\left(V\right)\left(1-s_k\right) - \gamma\left(V\right)s_k\right]\epsilon^k + \sqrt{\left(\delta\left(V\right)\left(1-s_k\right) + \gamma\left(V\right)s_k\right)N_{s,k}^{-1}\epsilon^k}\xi_{s,k}\,,$$

with $\phi_{s,k} = \epsilon^k$ and $N_{s,k} = N_s\epsilon^{\nu k}$, where $\gamma\left(V\right)$ and $\delta\left(V\right)$ are taken from the HHS model. Note that N_s, ν, M and $\epsilon < 1$ are free parameters. In order to fit the experimental results in Fig. 3, we set $N_s = 10^4, \nu = 0.5, M = 5$ and $\epsilon = 0.2$ so that $S_Y\left(f\right) \sim f^{-\alpha}$, with $\alpha \approx 1.4$ (the average measured value in [11]).

D External fluctuation sources

The work in [11] investigated isolated neurons under sparse spike stimulation with fixed amplitude, as discussed here. As explained in [48], under such stimulation the neuronal response can be very sensitive to small changes in excitability - both internal or external. Therefore, it is important to make sure that the observed non-stationary $f^{-\alpha}$ behavior is not generated by external fluctuation sources that may be present in the experimental setup (an in-vitro culture of cortical neurons).

For example, such external fluctuation sources may include temperature and ion concentration fluctuations, and fluctuations in the electrode-bath interface. These are Common Non-stationary Fluctuation (CNF) sources since they should affect all the neurons that are being stimulated (in the experiments of [11], several neurons were stimulated and recorded simultaneously). Additionally, although all synaptic connections were completely blocked, there is always the possibility that some other weak interactions (*e.g.*, gap junctions, ephaptic couplings, glia cells) between different neurons might affect the results.

In this section we explain the controls performed by [11], and perform additional analysis to corroborate them. These results suggest that the $f^{-\alpha}$ behavior is independent between neurons and is therefore generated internally.

D.1 Background - experimental controls

To rule out the presence of a CNF, [11] performed two main controls. First, they included in the analyses only cells which were relatively stable during the long experiment - for which the spike profile remained stable (Fig. 5C in [11]). In these cells the latencies and response patterns remained repeatable ([11], Fig. 9). Second, they examined the correlations between different (isolated) neurons in the same experiment, and found that they were rather low (see [11], Fig. 5E). Additional basic controls have been performed, but did not appear in the paper (personal communication). For example, to rule out fluctuations in the interface electrode-baths, the stability of impedance and the shape of the stimulation pulse were tested - verifying that indeed both have not changed much from the beginning to the end of the experiment. Lastly, we comment that the culture was kept under controlled temperature of 37°c.

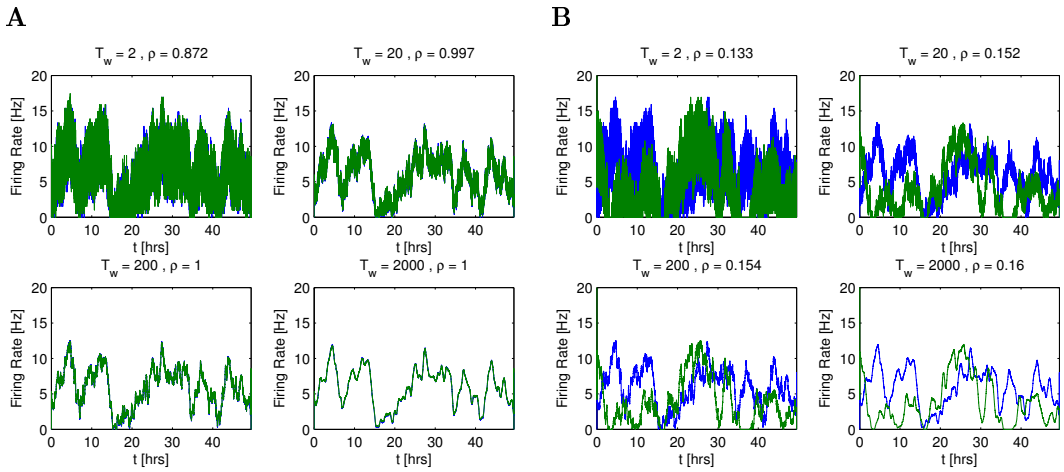

Figure 8: Firing rates for two (green and blue) simulated HHS neuron models with (**A**) common and (**B**) non-common current fluctuations in I_0, and for different averaging windows widths (T_w). Pearson correlation coefficients (see titles) are $\rho \geq 0.87$ when fluctuations are common and $\rho \sim 0.1$ when fluctuations are non-common.

D.2 Common non-stationary fluctuations

Recall that [11] found that correlations between different (isolated) neurons in the same experiment were rather low (a Pearson correlation coefficient of $\rho \sim 0.15$ or lower). If the source of the $f^{-\alpha}$ behavior in the experiment is a common noise source which affects several different neurons, one would expect these correlations to be much higher. To verify this is reasonable, we modeled the CNF as a random walk (symmetric diffusion process) in I_0, the amplitude of the injected current to the HHS model (*e.g.*, such a CNF may result from accumulating variations in the electrode interface). The step size parameter of the random walk was fitted so the magnitude of the response fluctuations would be qualitatively similar to the experimental results of [11], as can be seen in Fig. 8 (compare with Fig. 5D in [11]).

When the CNF was common (*i.e.*, the same realization of the CNF was used for two different simulations, Fig. 8A), the correlation coefficient ρ was typically very close to one, and always above 0.8 (it is not exactly one, since the model is stochastic). In contrast, when two simulations had different realizations of the CNF (*i.e.*, different sample paths, Fig. 8B) then the correlation coefficient between the firing rates in both simulations was $\rho \sim 0.15$, similarly to the experiment. Similar results were obtained when the fluctuations were added instead to the sodium conductance $\bar{g}_{\mathrm{Na}}$ (*e.g.*, resulting from CNF in the temperature, affecting the Q10 of the channel), or to the sodium Nernst potential V_{Na} (*e.g.*, resulting from a CNF in the temperature and sodium ion concentrations).

These simulations provide a strong indication that if indeed the $f^{-\alpha}$ behavior was generated by a CNF, this would result in strong correlations between the responses of different neurons in the culture - in contrast to the low correlations observed by [11].

D.3 Inter-neuronal interactions

Recall again that in [11] the neurons are synaptically isolated. Therefore, in our work we assumed that any interaction between neurons is negligible in comparison to the intrinsic neural dynamics and stimulation, as is commonly done when modeling neurons biophysically. There is additional evidence to suggest this assumption is reasonable. First, we note that the results reported in [11] do not seem to depend on the density of the neural culture, or on the number of neurons responding to stimulation (personal communication). If these interactions were important, we would expect this not to be the case. Moreover, the correlations between different neurons are low, as we mentioned in section D.2.

However, as explained in [42], even with such low correlations, significant interactions might be present. In order to check if there might be other indications to such interactions, we performed analysis, similar to [42], on an experiment from [11], where six different neurons where simultaneously stimulated and recorded (using a time bin of 0.05 sec, as the period of the stimulation). Similarly to [42], we measured $P_{\text{emp}}(\mathbf{x})$, the empirical binary 'word' frequency observed in the data in each stimulation (*e.g.*, if, after a stimulation, the first four neurons did not respond and the last two did respond, then the resulting 'word' is $\mathbf{x} = 000011$). Then we compared the empirical word probability $P_{\text{emp}}(\mathbf{x})$ with $\prod_i P_{\text{emp}}(x_i)$, the product of the empirical probability marginals. If the neurons are completely independent then we expect both to be very similar. This is indeed the case - as can be seen in Fig. 9 (compare with fig. 2a in [42]).

This indicates that interactions between neurons in the culture in [11] are rather weak, and supports our assumption that these interactions are negligible in comparison to the intrinsic neural dynamics and stimulation.

Acknowledgments The authors are grateful to O. Barak, N. Brenner, Y. Elhanati, A. Gal, T. Knafo, Y. Kafri, S. Marom, J. Schiller and M. Ziv for insightful discussions and for reviewing parts of this manuscript. The authors are also grateful to A. Gal and S. Marom for supplying the experimental data. The research was partially funded by the Technion V.P.R. fund and by the Intel Collaborative Research Institute for Computational Intelligence (ICRI-CI).

References

[1] *http://channelpedia.epfl.ch/.*

[2] B. P. Bean, *The action potential in mammalian central neurons.*, Nature Reviews Neuroscience, 8 (2007), pp. 451–65.

[3] C. Bédard, H. Kröger, and a. Destexhe, *Does the 1/f Frequency Scaling of Brain Signals Reflect Self-Organized Critical States?*, Physical Review Letters, 97 (2006), p. 118102.

[4] J. S. Bendat and A. G. Piersol, *Random Data Analysis and Measurement Procedures*, vol. 11, Wiley, New York, NY, 3rd ed., Dec. 2000.

[5] J. Beran, *Statistics for long-memory processes*, Chapman & Hall, New York, NY, 1994.

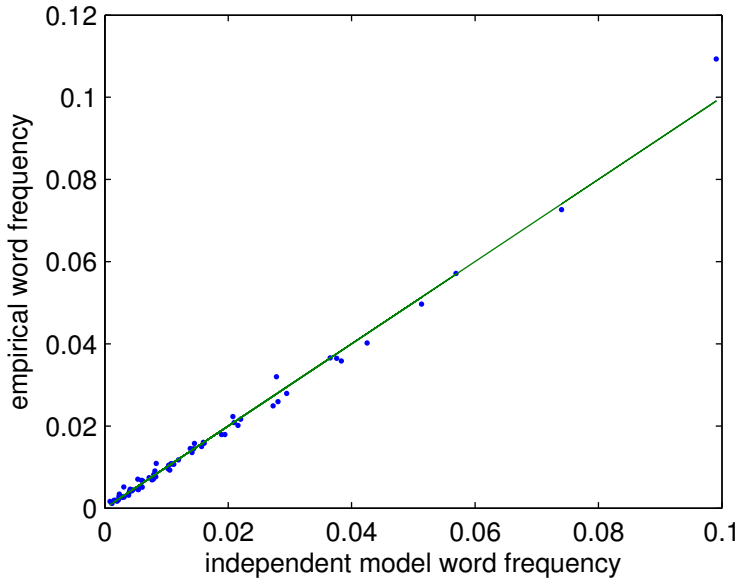

Figure 9: Binary word frequencies - empirical word frequency (the probability $P_{\text{emp}}(\mathbf{x})$) versus the independent model word frequency (a product of the marginal empirical probabilities $\prod_i P_{\text{emp}}(x_i)$) (blue dots are the words, and green line has slope one, for comparison). Both seem quite similar, indicating the the responses of different neurons are independent.

[6] W. K. Chandler and H. Meves, *Slow changes in membrane permeability and long-lasting action potentials in axons perfused with fluoride solutions*, The Journal of Physiology, 211 (1970), pp. 707–728.

[7] E. Davidson and M. Levin, *Gene regulatory networks.*, Proceedings of the National Academy of Sciences of the United States of America, 102 (2005), p. 4935.

[8] R. De Col, K. Messlinger, and R. W. Carr, *Conduction velocity is regulated by sodium channel inactivation in unmyelinated axons innervating the rat cranial meninges*, The Journal of Physiology, 586 (2008), pp. 1089–1103.

[9] D. Debanne, E. Campanac, A. Bialowas, and E. Carlier, *Axon Physiology*, Physiological Reviews, 91 (2011), pp. 555–602.

[10] I. A. Fleidervish, A. Friedman, and M. J. Gutnick, *Slow inactivation of Na+ current and slow cumulative spike adaptation in mouse and guinea-pig neocortical neurones in slices*, Journal of Physiology, 493 (1996), pp. 83–97.

[11] A. Gal, D. Eytan, A. Wallach, M. Sandler, J. Schiller, and S. Marom, *Dynamics of Excitability over Extended Timescales in Cultured Cortical Neurons*, Journal of Neuroscience, 30 (2010), pp. 16332–16342.

[12] A. Gal and S. Marom, *Entrainment of the intrinsic dynamics of single isolated neurons by natural-like input*, The Journal of Neuroscience, 33 (2013), pp. 7912–7918.

[13] A. Gal and S. Marom, *Self-organized criticality in single neuron excitability*, Physical Review E (In press), (2013).

[14] D. Gilden, T. Thornton, and M. Mallon, *1/f noise in human cognition*, Science, 267 (1995), pp. 1837–1839.

[15] D. T. Gillespie, *The chemical Langevin equation*, The Journal of Chemical Physics, 113 (2000), p. 297.

[16] G. C. Goodwin and R. L. Payne, *Dynamic system identification: Experiment design and data analysis*, Academic Press New York, New York, New York, USA, 1977.

[17] B. Y. Y. Grossman, I. Parnas, and M. E. Spira, *Differential conduction block in branches of a bifurcating axon*, The Journal of Physiology, 295 (1979), pp. 307–322.

[18] M. S. Grubb and J. Burrone, *Activity-dependent relocation of the axon initial segment fine-tunes neuronal excitability*, Nature, 465 (2010), pp. 1070–1074.

[19] B. Hille, *Ion Channels of Excitable Membranes*, Sinauer Associates, Sunderland, MA 01375, 3rd ed., 2001.

[20] A. L. Hodgkin and A. F. Huxley, *A quantitative description of membrane current and its application to conduction and excitation in nerve*, The Journal of physiology, 117 (1952), p. 500.

[21] M. S. Keshner, *Renewal process and diffusion models of 1/f noise*, PhD thesis, 1979.

[22] ——, *1/f noise*, Proceedings of the IEEE, 70 (1982), pp. 212–218.

[23] I. B. Levitan, *Modulation of ion channels by protein phosphorylation and dephosphorylation*, Annual Review of Physiology, 11 (1994), pp. 193–212.

[24] S. B. Lowen, L. S. Liebovitch, and J. A. White, *Fractal ion-channel behavior generates fractal firing patterns in neuronal models*, Physical Review E, 59 (1999), p. 5970.

[25] S. B. Lowen and M. C. Teich, *Fractal-based point processes*, 1st ed., 2005.

[26] B. N. Lundstrom, A. L. Fairhall, and M. Maravall, *Multiple timescale encoding of slowly varying whisker stimulus envelope in cortical and thalamic neurons in vivo.*, The Journal of Neuroscience, 30 (2010), pp. 5071–7.

[27] B. N. Lundstrom, M. M. H. M. H. Higgs, W. J. W. J. W. Spain, and A. L. Fairhall, *Fractional differentiation by neocortical pyramidal neurons*, Nature Neuroscience, 11 (2008), pp. 1335–42.

[28] E. Marder and J.-M. Goaillard, *Variability, compensation and homeostasis in neuron and network function.*, Nature Reviews Neuroscience, 7 (2006), pp. 563–74.

[29] S. Marom, *Neural timescales or lack thereof*, Progress in Neurobiology, 90 (2010), pp. 16–28.

[30] T. Musha and M. Yamamoto, *1/f fluctuations in biological systems*, in Proceedings of the 19th Annual International Conference of the IEEE Engineering in Medicine and Biology Society. 'Magnificent Milestones and Emerging Opportunities in Medical Engineering' (Cat. No.97CH36136), vol. 6, IEEE, pp. 2692–2697.

[31] B. Naundorf, F. Wolf, and M. Volgushev, *Unique features of action potential initiation in cortical neurons.*, Nature, 440 (2006), pp. 1060–3.

[32] M. Newman, *Power laws, Pareto distributions and Zipf's law*, Contemporary Physics, 46 (2005), pp. 323–351.

[33] H. Nishiyama, M. Fukaya, and M. Watanabe, *Axonal motility and its modulation by activity are branch-type specific in the intact adult cerebellum*, Neuron, 56 (2007), pp. 472–487.

[34] A. Oppenheim, A. Willsky, and S. Nawab, *Signals and systems*, Prentice Hall, Englewood Cliffs, NJ, 1983.

[35] P. Orio and D. Soudry, *Simple, fast and accurate implementation of the diffusion approximation algorithm for stochastic ion channels with multiple states*, PLoS ONE, 7 (2012), p. e36670.

[36] V. D. Paola, A. Holtmaat, G. Knott, S. Song, L. Wilbrecht, P. Caroni, K. Svoboda, and V. De Paola, *Cell type-specific structural plasticity of axonal branches and boutons in the adult neocortex.*, Neuron, 49 (2006), pp. 861–75.

[37] A. Papoulis and S. U. Pillai, *Probability, Random Variables, and Stochastic Processes*, McGraw-Hill New York, 1965.

[38] C. K. Peng, S. Havlin, H. E. Stanley, and a. L. Goldberger, *Quantification of Scaling Exponents and Crossover Phenomena in Nonstationary Heartbeat Time Series*, Chaos (Woodbury, N.Y.), 5 (1995), pp. 82–7.

[39] C. Pozzorini, R. Naud, S. Mensi, and W. Gerstner, *Temporal whitening by power-law adaptation in neocortical neurons*, Nature Neuroscience, 16 (2013), pp. 942–948.

[40] B. H. Repp, *Sensorimotor synchronization: a review of the tapping literature.*, Psychonomic bulletin & review, 12 (2005), pp. 969–992.

[41] P. M. Robinson, *Time series with long memory*, Oxford Univ Pr, New York, 2003.

[42] E. Schneidman, M. J. Berry, R. Segev, and W. Bialek, *Weak pairwise correlations imply strongly correlated network states in a neural population.*, Nature, 440 (2006), pp. 1007–12.

[43] I. A. Silver, J. Deas, and M. Erecinska, *Ion homeostasis in brain cells: differences in intracellular ion responses to energy limitation between cultured neurons and glial cells.*, Neuroscience, 78 (1997), pp. 589–601.

[44] P. J. Sjöström, E. A. Rancz, A. Roth, and M. Häusser, *Dendritic excitability and synaptic plasticity*, Physiological Reviews, 88 (2008), pp. 769 – 840.

[45] Y. Soen and E. Braun, *Scale-invariant fluctuations at different levels of organization in developing heart cell networks.*, Physical Review E, 61 (2000), pp. R2216–9.

[46] D. Soudry and R. Meir, *The neuronal response at extended timescales: a linearized spiking input-output relation*, under review.

[47] ——, *History-dependent dynamics in a generic model of ion channels - an analytic study*, Front. Comput. Neurosci., 4 (2010).

[48] D. Soudry and R. Meir, *Conductance-based neuron models and the slow dynamics of excitability*, Front. Comput. Neurosci., 6 (2012).

[49] O. Staub, I. Gautschi, T. Ishikawa, K. Breitschopf, A. Ciechanover, L. Schild, and D. Rotin, *Regulation of stability and function of the epithelial Na+ channel (ENaC) by ubiquitination.*, The EMBO Journal, 16 (1997), pp. 6325–6336.

[50] L. Ward and P. Greenwood, *1/f noise*, Scholarpedia, 2 (2007), p. 1537.